Emerging Applications of Atomic Layer Deposition for Lithium-Ion Battery Studies

Xiangbo Meng, Xiao-Qing Yang, and Xueliang Sun**

Lithium-ion batteries (LIBs) are used widely in today's consumer electronics and offer great potential for hybrid electric vehicles (HEVs), plug-in HEVs, pure EVs, and also in smart grids as future energy-storage devices. However, many challenges must be addressed before these future applications of LIBs are realized, such as the energy and power density of LIBs, their cycle and calendar life, safety characteristics, and costs. Recently, a technique called atomic layer deposition (ALD) attracted great interest as a novel tool and approach for resolving these issues. In this article, recent advances in using ALD for LIB studies are thoroughly reviewed, covering two technical routes: 1) ALD for designing and synthesizing new LIB components, i.e., anodes, cathodes, and solid electrolytes, and; 2) ALD used in modifying electrode properties via surface coating. This review will hopefully stimulate more extensive and insightful studies on using ALD for developing high-performance LIBs.

1. Introduction

With the constantly increasing worldwide need for energy, fossil-based fuels (coal, petroleum, and natural gas) as our main energy sources are rapidly being depleting, while their combustion is increasing the output of greenhouse gases and other pollutants in our environment.[1] Therefore, there is an urgent need to seek renewable clean energy sources as alternatives. Today's principal candidates for these roles are solar and wind energy.[1–3] Unfortunately, the ability of either one to satisfy these energy needs is limited by geographical considerations, and nor can they be continuously and smoothly operated. Energy security affects our mobility, prosperity, and daily comfort.[4] Thus, energy storage is a critical issue in supporting the extensive applications of these two renewable energy sources.[2]

Batteries are used widely to store electrical energy in the form of chemical energy.[5] Lithium-ion batteries (LIBs) now are the dominant type of rechargeable batteries for various consumer electronic applications, reflecting their high energy and power density over other types of batteries.[3,5] A LIB cell conventionally consists of a carbon anode (negative electrode, e.g., graphite), a lithium metal oxide cathode (positive electrode, e.g., $LiCoO_2$), an electronically insulating separator, and an ionically conductive electrolyte to transfer lithium ions between the two electrodes. The electrolytes can be a liquid, a gel or solid polymer, or an inorganic solid.[5] In most cases, LIBs use liquid electrolytes containing a lithium salt, such as $LiPF_6$, $LiBF_4$, $LiBC_4O_8$ (LiBOB), and $Li[PF_3(C_2F_5)_3]$ (LIFAP), that is dissolved in a mixture of organic alkyl carbonate solvents, such as ethylene, dimethyl, diethyl, and ethyl methyl carbonate (i.e., EC, DMC, DEC, and EMC, respectively).[6] An external connection between the two electrodes induces a spontaneous flow of electrons from the anode to the cathode, due to their different chemical potentials dictated by the materials chemistry.[7] As so-called the rocking chair batteries, LIBs rely on the shuttling of lithium-ions back and forth between the two electrodes during charge-discharge cycles. The materials chemistry governs both cell voltage and capacity.[7,8] LIBs were first commercialized in 1991 by Sony Corporation.[7,9] Currently, LIBs provide a voltage of the order of 4 V, and specific energy ranging from 100 to 150 Wh/kg.[10] LIBs have three main application domains:[3,5,6] portable electronics; transport; and, stationary storage. So far, the first usage is the best developed and largest in terms of the number of units generated; the other two are expected to be boosted in the coming years.[5] At present, the construction of large stationary batteries as centralized facilities is still expensive.[3] The most notable scaled-up application is for hybrid electrical vehicles (HEVs), plug-in HEVs, and pure EVs.[6] Unfortunately, conventional LIBs (e.g., $C/LiCoO_2$ batteries) suffer from a series of problems for transportation use, i.e., cost, safety, cell energy density (voltage × capacity), rate of charge-discharge, and service life,[10,11] whose roots lie in the anodes, cathodes, electrolytes, and the interrelations between them.[12,13] More specifically, LIBs must be able to operate at realistic temperatures (ranging from –46 to +66 °C) with 5000 charge-discharge cycles and a 15-year calendar life.[14] However, these requirements still challenge current LIB technologies. Therefore, intensive research is being conducted worldwide on new materials for the next generation of LIBs.

Since Poizot et al.[15] reported that some nanostructured materials are more advantageous than bulk materials for electrodes, a large variety of nanomaterials and their composites

Dr. X. Meng, Dr. X. Sun
Department of Mechanical and Materials Engineering
The University of Western Ontario, London
ON N6A 5B8, Canada
E-mail: xsun@eng.uwo.ca
Dr. X. Meng, Dr. X.-Q. Yang
Chemistry Department
Brookhaven National Laboratory
Upton, NY, 11973, USA
E-mail: xyang@bnl.gov

DOI: 10.1002/adma.201200397

have been investigated, as detailed in many reviews.[3,6,8,16–26] The benefits offered by nanomaterials[15,17,21,25] include the following: (1) improved cycling life due to better accommodating the strain of lithium insertion-disinsertion; (2) new reactions not possible with bulk materials; and, (3) higher charge-discharge rates due to greater electrode/electrolyte contact area and shorter path length for transporting both electrons and lithium ions. However, associated with these benefits, nanoelectrodes carry some disadvantages, such as undesirable reactions due to their high surface area, inferior packing leading to lower volumetric energy densities, and more complex synthesis. Thus, researchers have also been seeking solutions from electrolytes/separators[27–32] and other strategies to modify electrodes and electrolytes.[33–39] Among the choices, surface coating of the electrodes[20,21,34–39] proved an effective venue for improving the performance of LIBs and it encompasses different types of coating materials depending on the nature of electrodes. For example, carbon coating was widely adopted for both anode and cathode materials in order to enhance electrical conductivity, buffer volume change, or stabilize solid electrolyte interphase (SEI) films.[20,21,34,36,39] In addition, the coatings of metals (e.g., Ag), metal oxides (e.g., Al_2O_3, SnO_2, ZrO_2, MgO, and ZnO), and other materials were also demonstrated to be beneficial for the better performance of LIBs.[20,21,34–38]

In addressing these various challenges facing LIBs, a technique called atomic layer deposition (ALD) is attracting great interest that is ascribed to its multifunctional capabilities and unique characteristics. Recent advances demonstrated that by using ALD not only can researchers accurately design various new high-performance LIB components, including anodes, cathodes and electrolytes, but they are also able to modify the properties of electrode materials with ultrathin coating films. Stimulated by ALD's extensive applications in LIBs, we summarize here the recent progress. This review covers five parts in total. Following this introductory section, in the second section we present an illustrative description of the mechanisms of ALD and a comprehensive survey of its unique characteristics. We then highlight and detail the applications of ALD for LIBs in two separate sections: the precise design and synthesis of novel LIB components by ALD are discussed in the third section, and then recent applications of ALD in modifying both anodes and cathodes are outlined in the fourth part. As a concluding remark, the fifth section summarizes the successes of ALD in LIBs and, in particular, gives outlooks and expectations for future studies. With this approach, we are hoping to provide readers with an integrated picture, and to boost more extensive studies on the applications of ALD for LIB research.

2. Fundamentals of ALD

2.1. Mechanisms

ALD is a vapor-phase deposition process, that first emerged in 1970s and credited to Suntola and co-workers.[40] Its initial application was limited to the synthesis of II-VI and III-V compounds for thin film electroluminescent (TFEL) display

Xiangbo (Henry) Meng is a Research Associate in Dr. Yang's group in the Chemistry Department at Brookhaven National Laboratory (BNL, USA), and receives the Canadian NSERC Postdoctoral Fellowship. He earned his first PhD in Chemical and Biochemical Engineering in 2008 and his second PhD (supervised by Dr. Sun) in Mechanical and Materials Engineering in 2011, both at The University of Western Ontario, Canada. He has a range of research interests in particle technology, pollution control, nanotechnology, and clean energy devices. His current research at BNL focuses on the development of new battery materials using ALD and the characterization of lithium-ion batteries using synchrotron-based techniques such as in situ X-ray diffraction and adsorption.

Xiao-Qing Yang is a Scientist in the Chemistry Department at BNL. He got his PhD in Physics at the University of Florida in 1986. Since then he has been working at BNL, and his research focuses on materials for lithium-ion batteries and the development of new characterization tools for battery materials using a series of synchrotron-based techniques. He has served as organizer or co-chairman for international conferences such as the Technical Conference of the Sixth China International Battery Fair (CIBF2006, Beijing, China) and the 2007 International Battery Materials Association Meeting (IBA2007, Shenzhen, China). He was elected Secretary General of the 14th International Meeting of Lithium Batteries (IMLB2008).

Xueliang (Andy) Sun is a Professor and Canada Research Chair at the University of Western Ontario, Canada. He received his PhD in Materials Chemistry in 1999, followed by work as a postdoctoral fellow at the University of British Columbia, and as a Research Associate at l'Institut national de la recherche scientifique (INRS), Canada. His current research interests are associated with the synthesis of nanomaterials for electrochemical energy storage and conversion. His focus is on the design and synthesis of various 1D nanostructures and their composites as electrocatalysis and catalyst supports in fuel cells and as anodes and cathodes in lithium-ion and Li-air batteries.

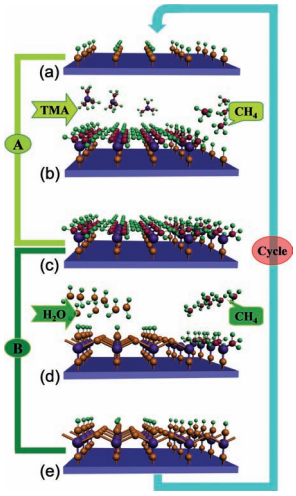

Figure 1. A model ALD process for depositing Al_2O_3 using TMA and water as precursors: (a) the initial substrate covered by hydroxyl groups; (b) TMA molecules reacting with hydroxyl groups, leading to a new intermediate layer; (c) the substrate covered with a newly created intermediate layer; (d) H_2O molecules reacting with the intermediate layer, leading to new hydroxyl groups, and; (e) the substrate again covered by hydroxyl groups.

devices.[41,42] Thereafter, progress in ALD was slow. Presently, concurred with the demanding needs in scaling complementary metal-oxide-semiconductor (CMOS), ALD is undergoing a renaissance starting from the beginning of the 21st century. In contrast to its traditional counterparts, such as chemical vapor deposition (CVD) and physical vapor deposition (PVD) that are dominated by the supply of precursor sources, ALD is a surface-controlled process wherein the growth of films is dictated by two self-terminating gas-solid surface reactions. To demonstrate the mechanisms of ALD processes, we illustrate in **Figure 1**, a classical ALD process for the binary compound Al_2O_3. Two precursors are exclusively required for a binary ALD. The most successful ALD process of Al_2O_3 (ALD-Al_2O_3) uses trimethylaluminum (TMA) and water as precursors, as shown in Figure 1. In a CVD process, the TMA and water reaction is described by an overall reaction:[43]

$$2Al(CH_3)_3 + 3H_2O \rightarrow Al_2O_3 + 6CH_4 \quad (1)$$

In comparison, the ALD-Al_2O_3 proceeds with two half-reactions, suggested as follows:[43]

$$AlOH^* + Al(CH_3)_3(g) \rightarrow Al-O-Al(CH_3)_2^* + CH_4(g) \quad (2A)$$

$$Al-O-Al(CH_3)_2^* + 2H_2O(g) \rightarrow Al-O-Al(OH)_2^* + 2CH_4(g) \quad (2B)$$

where the asterisks (*) designate species attached on substrates by chemisorption and (g) the gaseous phase of precursors or byproducts. In practice, an ALD-Al_2O_3 process includes four repetitive steps: (1) a supply of the aluminum source precursor TMA to induce a surface reaction (i.e., 2A, Figure 1(b)) with the reactive sites (e.g., -OH, Figure 1(a)) on a substrate or on a former-deposited film, and thereby to form an intermediate layer (i.e., -$Al(CH_3)_2$, Figure 1(b) and (c)) with the release of CH_4 as the byproduct; (2) a purging phase following the self-terminated reaction 2A to evacuate the oversupplied non-reacted TMA and the gaseous byproduct CH_4; (3) a supply of an oxygen precursor H_2O to start another surface reaction (i.e., 2B, Figure 1(d)) with the reactive groups (i.e., -CH_3) of the intermediate layer and to produce the target product Al_2O_3 as well as new reactive sites (i.e., -OH, Figure 1(e)); (4) another purging phase to evacuate the oversupplied non-reacted precursor H_2O and the gaseous byproduct CH_4. These four steps are repeatable. Thus, ALD operates cyclically and proceeds in a layer-by-layer manner.

It should be emphasized that, for an ALD process as illustrated in Figure 1, there are three key parameters jointly determining the deposition features. They are substrate, temperature, and precursor. In the first place, as shown by Figure 1, the substrate must initially be functionalized with reactive sites.[44] The first half-reaction relies on the interaction between the surface reactive sites and the first precursor. The reaction terminates with a new created layer when the surface reactive sites are saturated. In other words, the gas-solid reaction is by nature self-limiting. The new layer provides reactive sites for a following half-reaction while the oversupplied precursor and by-products are purged by a vacuum system. Similarly, the second half-reaction creates another new layer with new functional groups for the following reactions and is also self-terminating. In fact, the two half-reactions combine to produce the target material in a well-controlled growth manner at the atomic level. In fact, both the initial coverage of reactive sites and the inherent properties of a substrate affect the growth of deposited materials. Temperature, in the second place, is another crucial factor for sustaining ALD characteristics. As discussed, ALD performs in a self-limiting manner and therefore it requires the adsorption of precursors to be chemisorption rather than physisorption.[45] Consequently, the lowest temperature allowable for ALD should be able to minimize physisorbed ligands. On the other hand, a suitable ALD temperature should not decompose any precursor. Otherwise, the deposition will proceed in a CVD manner other than an ALD one. In contrast to CVD, ALD typically proceeds at much lower temperatures, even down to room temperature (RT).[46] There may exist a range of temperatures in which the growth of ALD is comparatively constant, called the ALD window. Thirdly, ALD precursors should provide sufficient vapors, and their concentrations in the gaseous phase must exceed a threshold value to saturate all the adsorption sites on a substrate[47] in order to achieve continuous monolayer coverage. Initially, the fractional coverage increases linearly with precursor's partial pressure, but then levels off to 100% once a threshold pressure is exceeded. This threshold must be determined experimentally from deposition rates and film properties, and usually chemisorption occurs on time scales of tens of milliseconds.[48] It is worth noting that precursors take effect on the ALD growth, closely related to their properties. Furthermore, complete purging of oversupplied precursors and by-products is also critical for avoiding continuous processes (e.g., CVD and PVD) and for accurately controlling the ALD growth per cycle (GPC). Hence, the purging flow rates must be sufficiently high to reduce the concentrations of oversupplied precursors and byproducts to a trace level after

each half reaction,[47] or the purges have to be elongated. In general, a mechanical pump is used to maintain the vacuum of an ALD system, which is essential for the supply of precursors and the following purge of unreacted precursors and byproducts. Typically, system pressure of ALD is of the order of 0.1–1 Torr, a medium value compared to those for PVD and CVD. In addition, a carrier gas usually is required, such as nitrogen or argon.

2.2. Characteristics

The unique reaction mechanisms and operation of ALD, as discussed above, imparts several distinct advantages over its vapor-phase counterparts (e.g., CVD and PVD) and even solution-based methods, as discussed below.

2.2.1. Low Growth Temperature

One of main features of ALD, especially in comparison to CVD, is its much lower growth temperature (typically less than 400 °C, versus 600–1000 °C for CVD). In particular, ALD deposits many materials at temperatures below 100 °C, even down to RT. Gasser et al. in 1994 conducted the first ALD experiment at RT, depositing SiO_2 from $Si(NCO)_4$ and water.[46] Later in 1997, Luo et al.[49] deposited CdS on ZnSe (100) at RT in an ultra-high-vacuum ALD system using $Cd(CH_3)_2$ and H_2S as precursors. Almost simultaneously, Klaus et al.[50] at University of Colorado discovered that ALD-SiO_2 could be performed at RT by catalyzing the surface reactions of $SiCl_4$ and water with pyridine (C_5H_5N), though most ALD processes to date are catalyst-free. Other metal oxides deposited by ALD at or around RT include B_2O_3,[51] Al_2O_3,[52,53] TiO_2,[53] ZnO,[54] ZrO_2,[55] and SnO_2,[56] etc. In addition, some metals such as Cu[57] and Pd[58] were also deposited by ALD at temperatures below 100 °C. This benefit is particularly attractive for coating heat-sensitive materials, such as polymers or biomaterials.

2.2.2. Atomic-Scale and Stoichiometric Deposition

Due to its layer-by-layer self-limitation, ALD's other advantage lies in enabling the precise control of the deposited films at the atomic level. This character assures the superiority of ALD over CVD, PVD, and solution-based methods. In general, the GPCs of ALD are at the level of angstroms (typically less than 2 Å/cycle), jointly determined by the precursors, temperatures, and substrates employed. For example, the GPC for the ALD-Al_2O_3 of using TMA and water reached the maximum of 1.33 Å/cycle in the range 100–125 °C, while GPC values were less at higher or lower temperatures.[52] In contrast, the ALD-Al_2O_3 of using $Al(CH_3)_2Cl$ and water reached a maximum GPC of approximately 0.8 Å/cycle in a narrow temperature range from 180 to 250 °C,[59] while the ALD-Al_2O_3 of using $(CH_3)_2(C_2H_5)N{:}AlH_3$ and water resulted in a much higher GPC of 2.5 nm/cycle under growth temperatures less than 200 °C.[60] Noteworthily, in attempting to overcome the deposition slowness of the traditional ALD, Hausmann et al.[61] at Harvard University developed a pair of precursors, TMA and tris(tert-butoxy)silanol [$(Bu^tO)_3SiOH$], that realized the rapid deposition of SiO_2 with a GPC of 12 nm/cycle at temperature ranging from 200 to 300 °C. However, such cases are rare in ALD processes.

In addition to the precise control on GPC, ALD is also capable of tuning the compositions of deposited materials. As a whole, the ALD-deposited materials are stoichiometrically close to their theoretic values, although growth temperatures and precursors may exert some influence. Using Rutherford backscattering spectrometry (RBS), for example, Groner et al.[52] demonstrated that the O/Al ratios of the ALD-Al_2O_3 from TMA and water are close to 1.50 in the temperature range 33–177 °C, varying from 1.34 to 1.70. They also pointed out that there is no systematic trend with growth temperatures. Using time-of-flight elastic recoil detection analysis (TOF-ERDA), Niinistö et al.[62] studied the ALD of gadolinium oxide films, reporting that, using $Gd(thd)_3$ and O_3 as ALD precursors, the resultant Gd/O ratios are lower than the theoretic value of 0.67 but increase from 0.41 to 0.55 with temperatures increased from 225 to 350 °C. In contrast, $(CpCH_3)_3Gd$ and water as ALD precursors generated higher Gd/O ratios rising from 0.57 to 0.64 as temperatures increased from 150 to 250 °C. Furthermore, Kukli et al.[63] demonstrated that the ALD-HfO_2 yields stoichiometric dioxides when deposition is at 300 °C with $HfCl_4$ or HfI_4 and water as precursors. Thus, suitable choices of ALD parameters are crucial for precisely controlling both the GPCs and the composition of deposited films.

2.2.3. Excellent Uniformity and Conformality

Another advantage from ALD's unique mechanisms is the excellent uniformity and conformality of deposited films over those generated by CVD, PVD, and solution-based methods. Atomic force microscopy (AFM) showed that, for instance, the ALD-Al_2O_3 on flat substrates has a surface roughness of 1–3 Å for a deposition in the range 200–560 Å.[47,64,65] A much smaller surface roughness of 0.7 Å was even reported by Lee et al.[66] Apart from this uniformity, ALD also offers non-planar substrates with highly conformal films. Over the past decade, there has been a dramatically increasing number of reports on various conformal nanostructures prepared by ALD. Some representative ones are exemplified in **Figure 2**, such as the layered Al_2O_3-ZnO nanolaminates on Si substrates (Figure 2(a)),[67] SiO_2-coated TiO_2 composite nanoparticles (Figure 2(b)),[68] hollow TiO_2 nanoribbons (Figure 2(c)),[69] coaxial HfO_2 nanotubes (Figure 2(d)),[70] three-layered discontinued TiO_2 three-dimensional (3D) nanofilms (Figure 2(e)),[71] and, complex 3D Al_2O_3 nanostructures (Figure 2(f)).[72]

In addition, researchers using ALD have so far synthesized a large variety of materials ranging from inorganic to organic materials. Puurunen[45] made a comprehensive and thorough summary on ALD successes before 2005. Much progress on different classes of ALD-synthesized materials was reported since then, well documented in many reviews. Some recent summaries focused on introducing novel nanostructures and potential applications related to ALD, for example, those written by Knez et al.,[73] Kim et al.,[74] and George.[75] Now, the applications of ALD are widening, not just its initial uses for semiconductors. Among the new trends for ALD, there is increasing interest in employing ALD for energy conversion and storage such as fuel cells, solar cells, and LIBs, owing to its impressive superiorities

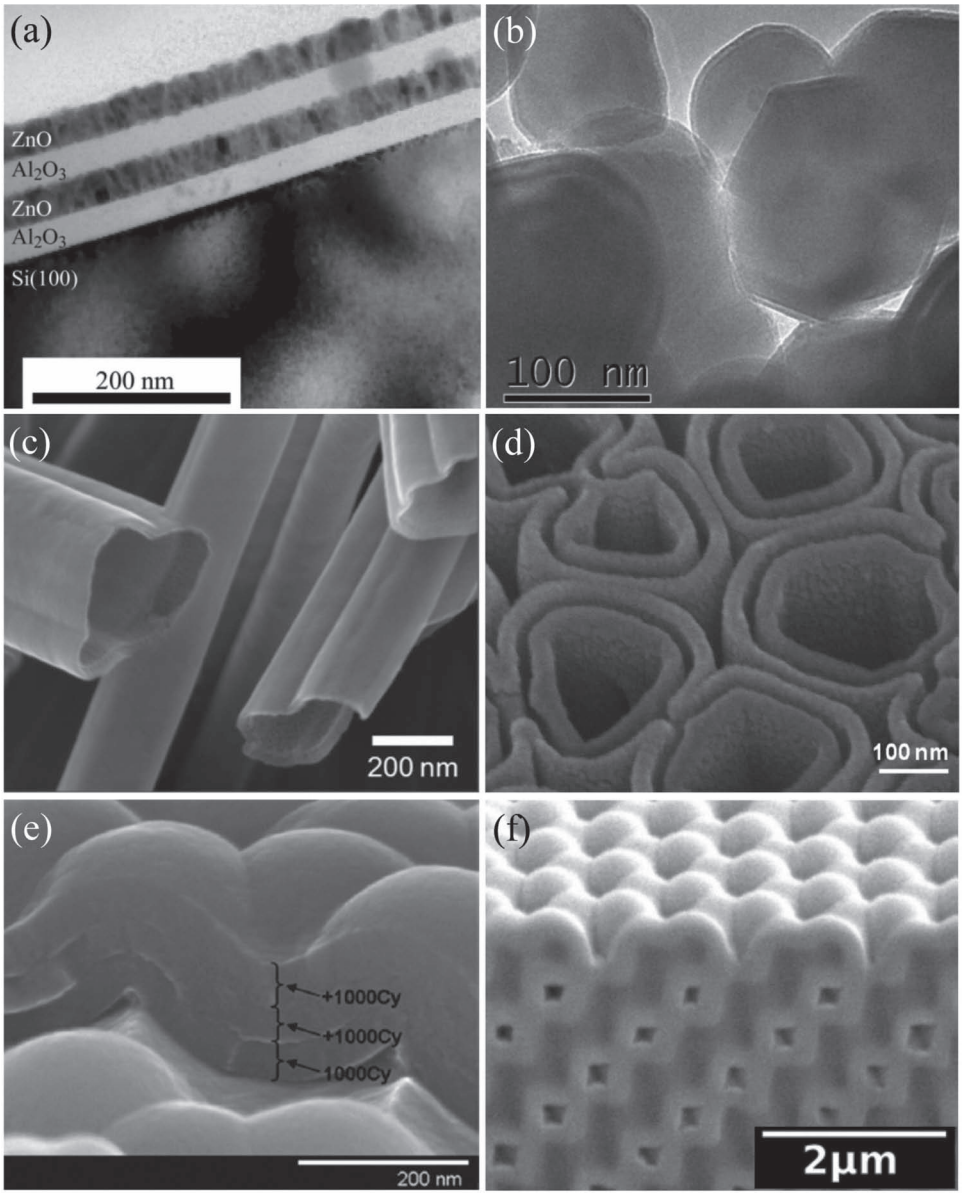

Figure 2. Various nanostructures fabricated by ALD: (a) the layered Al_2O_3-ZnO nanolaminates on Si substrates. Reproduced with permission.[67] Copyright 2002, Elsevier. (b) SiO_2-coated TiO_2 composite nanoparticles. Reproduced with permission.[68] Copyright 2010, American Chemical Society. (c) Hollow TiO_2 nanoribbons. Reproduced with permission.[69] Copyright 2010, Institute of Physics. (d) Coaxial HfO_2 nanotubes. Reproduced with permission.[70] Copyright 2010, American Chemical Society. (e) Three-layered discontinued TiO_2 3D nanofilms. Reproduced with permission.[71] Copyright 2010, American Chemical Society. (f) Complex 3D Al_2O_3 nanostructures. Reproduced with permission.[72] Copyright 2009, The Royal Society of Chemistry.

to other techniques. In this review, we focus on the emerging applications of ALD for high-performance LIBs.

3. Novel Battery Components Fabricated via ALD

3.1. Anodes

In conventional LIBs, carbon materials are exclusively used as anodes while lithium metal oxides $LiMO_2$ (M = Co, Ni, Mn, e.g., $LiCoO_2$) act as cathodes. In most cases, the liquid electrolyte employed is $LiPF_6$ in EC-DMC.[10] This configuration of C/($LiPF_6$ in EC-DMC)/$LiMO_2$ operates via a process:[6,10]

$$yC + LiMO_2 \leftrightarrow Li_xC_y + Li_{(1-x)}MO_2,$$
$$x \approx 0.5,\ y = 6,\ \text{and voltage} \approx 3.7\ \text{V at } 25\ ^\circ\text{C} \quad (3)$$

wherein lithium ions reversibly insert and extract between the two electrodes with the concomitant removal and addition of electrons. The carbon anodes have a limited specific theoretical capacity of 372 mAh/g.[6,17,23,25] Additionally, carbon materials suffer from capacity degradation due to irreversible side reactions that occur at the electrode/electrolyte interface between

Table 1. Nanostructured anode materials generated by ALD.

Materials	Precursor A	Precursor B	Temp. [°C]	Substrates	Nanostructures	Ref.
TiO_2	$TiCl_4$	H_2O	100–400	AAO	NT-A	[78–84]
			150	NC	NT-N	[85]
	TiI_4	H_2O	200	Al-NRd	NRd-A	[77]
			300	GNS	3D-N	[86]
	$Ti(NMe_2)_4$	H_2O	150	TMV	NT-A	[87]
	$Ti(O^iPr)_4$	H_2O	70–160	AAO	NT-A	[88,89]
			80–140	PC	NT-A	[88,90]
			150–250	GNS	3D-N	[91]
			35	TMV	NT-N	[53]
		NH_3	140	Peptide	NRb-N	[69,92]
		NH_3+O_2	140	Peptide	NRb-N	[93]
Fe_2O_3	$Fe(Cp)_2$	O_2	400	AAO	NT-A	[94]
			350	CNT	NT-N	[95]
	$Fe_2(O^tBu)_6$	H_2O	130–170	AAO	NT-A	[96]
ZnO	$Zn(C_2H_5)_2$	H_2O	40–200	CNT	NT-N	[97–99]
			200	AAO	NT-A	[100]
			250	AAO	NT-A, NRd-A	[101]
			150	NC	NT-N	[85]
SnO_2	$SnCl_4$	H_2O	200–400	AAO	NT-A	[102]
			200–400	CNT	NT-N	[103]
			200–400	GNS	3D-N	[104]
	$C_{12}H_{24}O_4Sn$	O_2	100	PAN-NF	NT-N	[105]
	$Sn(OCMe_3)_4$	AcOH	75–250	CNT	NT-N	[106]
	$C_{12}H_{26}N_2Sn$	H_2O_2	50–250	–	NT-A	[56]

lithium ions, the solvent, and the anode surface during charge-discharge cycles.[12,76] As such, better alternatives have been sought in the past decade. Lithium alloys, such as lithium-silicon (Li-Si) and lithium-tin (Li-Sn), are promising to provide higher specific capacity than carbon materials with a theoretic capacity of 4000 and 990 mAh/g, respectively.[6,10] Unfortunately, the lithium alloys undergo a large volume expansion-contraction (300–400%) during charge-discharge cycles, leading to mechanical stresses and thereby to the resultant disintegration of the anodes with subsequent failure.[6,10] Because of these issues with carbon and metallic anodes, metal oxides (e.g., TiO_2, MnO_2, Fe_2O_3, Co_3O_4, and SnO_2) and other compounds are being investigated as alternatives.[6,10,15,17,21,23,25] Among them, TiO_2 and lithium titanium oxide ($Li_4Ti_5O_{12}$, LTO) are especially attractive, even considering their disadvantages of relatively low specific capacity (335 mAh/g for TiO_2 and 175 mAh/g for LTO), and of relatively high potential levels (1.2–2.0 V vs. Li^+/Li).[6,10] Their common benefits include a negligible volume change, no electrolyte decomposition, no SEI formation, and thereby better safety and cycleability.[6,10,23]

3.1.1. Nanostructured Anode Materials via ALD

ALD is very successful for fabricating 2D planar films of metals and metal oxides, as detailed by Puurunen.[45] Many are potential anode materials, such as Si, MnO_x, Fe_2O_3, CoO_x, NiO, ZnO, and SnO_2. At that time, only a few nanostructures made via ALD were reported. In the past several years, a large number of nanostructured materials were developed by ALD, as we summarized in **Table 1**. In particular, electrochemical testing showed that these nanostructured materials are very favorable as candidate anodes for LIBs. As ascribed to the ALD's surface-controlled features, the resulting nanostructures are predominantly determined by their substrates. Mainly, three types of substrates are employed: porous templates, carbon-based materials, and biological materials. The first class includes anodic aluminum oxide (AAO) and polycarbonate (PC) templates, the second one encompasses polyacrylonitrile nanofibers (PAN-NF), carbon nanotubes (CNTs), and graphene nanosheets (GNS), and the last one covers nanocellulose (NC), tobacco mosaic virus (TMV), and peptides. Other substrates such as Al nanorods (Al-NRd)[77] were used in a few.

Based on the different substrates, a variety of nanostructures were fabricated by ALD, such as nanotube arrays (NT-A), nanotube networks (NT-N), nanoribbon networks (NRb-N), nanorod arrays (NRd-A), and 3D networks (3D-N). **Figure 3** schematically illustrates these main strategies and the resultant nanostructures. A traditional but typical way to produce nanotube arrays is based on AAO templates, as illustrated in Figure 3(a). In fact, this route is applicable for PC templates, that differs from the

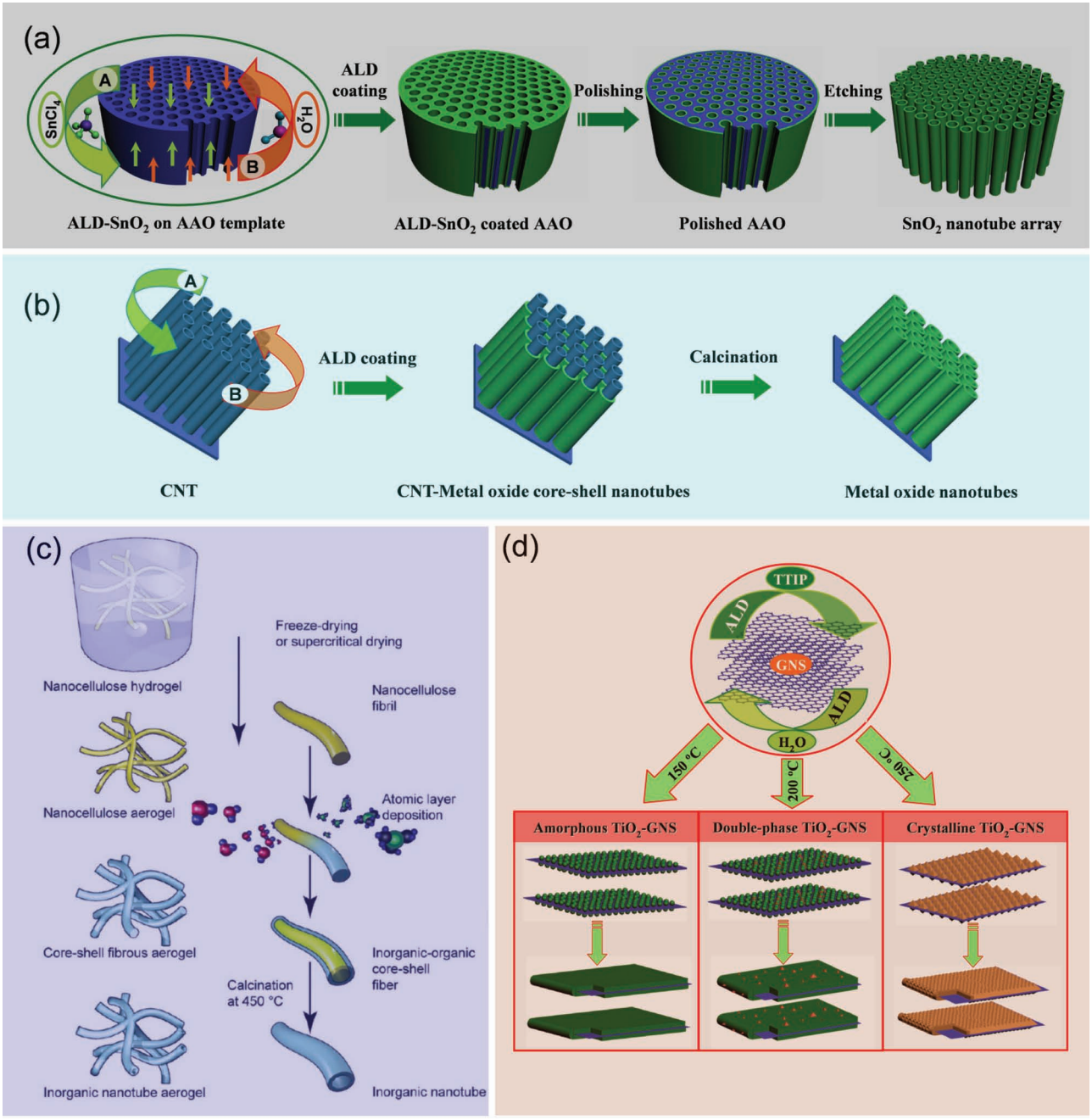

Figure 3. Main ALD strategies for fabricating nanostructured materials: (a) the strategy for nanotube arrays using AAO, exemplified by the fabrication of SnO_2 nanotubes. Reproduced with permission.[102] Copyright 2011, The Royal Society of Chemistry. (b) the strategy for nanotubes using CNTs. (c) the strategy for 3D networks of nanotubes based on nanocellulose aerogel. Reproduced with permission.[85] Copyright 2011, American Chemical Society. (d) the strategy for 3D nanostructures based on GNS, exemplified by ALD-TiO_2 on GNS.

former only in the etching process. Usually, sodium hydroxide (NaOH) or potassium hydroxide (KOH) is used to remove AAO while chloroform ($CHCl_3$) is employed to dissolve PC.[88] In addition, AAO is thermally stable while PC is suitable only for low temperature (<140 °C) ALD processes.[88] Another idea for obtaining nanostructures via ALD relies on 1D substrates such as nanotubes, nanofibers, nanoribbons, and nanorods, as is illustrated with CNTs in Figure 3(b). Depending on the pristine arrangement of substrates, the resultant nanostructures can be aligned arrays or networks of these 1D structures. In many cases, post-calcination is used to remove the core substrates, to improve the crystallinity of the synthesized nanostructures, or to reach both of them. Besides these two classes of substrates, a new strategy for using ALD is based on biological substrates including NC, peptide, and TMV. The low temperatures (<150 °C) of ALD favor these practices. As shown in Figure 3(c),

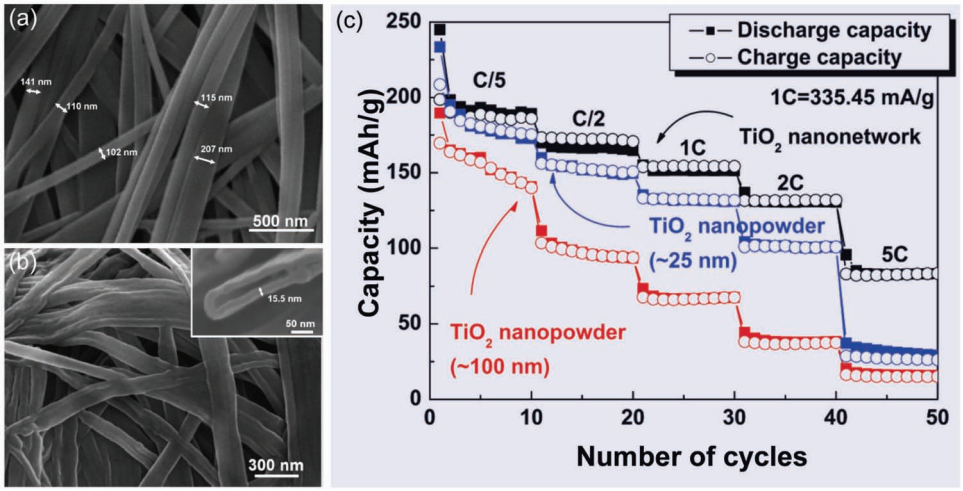

Figure 4. SEM images of (a) the peptide template and (b) the network of TiO_2 nanoribbons (inset: magnified image of cross sectional TiO_2 hollow nanoribbon), and; (c) rate capability for the TiO_2 network, and the 25 nm and 100 nm nanoparticles from C/5 to 5C in 10 cycles. Reproduced with permission.[93] Copyright 2009, American Chemical Society.

researchers[85] demonstrated ALD-TiO_2 and ZnO on NC aerogel that adopted a nanotube network configuration after calcination. Similarly, other researchers also developed hollow nanoribbon networks (Table 1). The most recent nanostructures from ALD are based on GNS. Graphene has attracted much attention since its discovery in 2004.[107] The reasons lie in a series of exceptional properties, such as high electric conductivity[108] and specific surface area.[109] Thus, expectedly, graphene-based nanocomposites will offer better performance in many applications. Using solution-based methods, for example, researchers developed several graphene-based metal oxides showing higher capacities, rate capabilities, and stability than pure metal oxides or graphene in LIBs.[110,111] Our recent work,[91] as illustrated in Figure 3(d), demonstrated that ALD is capable of depositing TiO_2 on GNS. In particular, our work highlighted some extra benefits that ALD provides in tuning the morphology and crystallinity of the deposited materials. Similar contributions were also reported with ALD-SnO_2.[102–104]

Seemingly, based on the above discussion, ALD offers versatile routes and a series of advantages for designing and synthesizing anode materials of LIBs. Impressively, it was also experimentally demonstrated that these novel nanostructures are effective for enhancing the electrochemical performance of LIBs.

3.1.2. High Performance of ALD Nanostructured Anodes

Previously, various vapor-phase and solution-based methods were used extensively for synthesizing novel anode materials of high performance, as described in several reviews.[15,22,23,25] Only recently was ALD reported as a new tool for developing anode materials (Table 1), featuring its high preciseness and tunability in the resultant structures, compositions, and growth of the deposited materials. Partially due to their late emergence, the ALD-produced anode materials were electrochemically tested only in a few cases, including TiO_2 and SnO_2, but they showed very promising performance in LIBs.

In the case of TiO_2, three different nanostructures were investigated and they commonly showed better performance as LIB anodes. The first experiments were conducted by Kim et al.[93] Applying ALD on a biotemplate of an assembly of peptides (**Figure 4** (a)), they deposited a layer of amorphous TiO_2 layer on the template at 140 °C. The as-synthesized materials were heated at 400 °C for 1 h to remove the biotemplate, leaving to a 3D network of crystalline anatase TiO_2 hollow ribbons (Figure 4(b)). Used as anode, this 3D network of anatase TiO_2 ribbons showed higher specific capacity, rate capability, and cycleability than did two TiO_2 nanoparticles (25 and 100 nm in size, respectively). In clear contrast to the rate capability of the TiO_2 nanoparticles, as illustrated by Figure 4(c), the TiO_2 network retains its superior rate capability as the current density increases by 25 times. The difference between the network and the two nanoparticles increases with the current rate. In another work, a different nanostructure of ALD-TiO_2 also demonstrated with high performance. Gerasopoulos et al.[87] developed a 3D nanostructure of TiO_2 on Ni-coated TMV (Ni-TWV). The deposited TiO_2 was amorphous and transferred to the anatase phase with post-annealing. The ultimate anatase TiO_2-(Ni-TMV) core-shell structure (**Figure 5**(a) and (b)) as anode showed a much higher specific capacity of 180–185 mAh/g than the one (90 mAh/g) of TiO_2 nanofilms (of comparable thickness but without TMV on steel substrates) at a current rate of 147mA/g (Figure 5(c)). It was also found that the TiO_2-(Ni-TMV) anode sustains its 3D structure after electrochemical testing. Furthermore, the differences between the 3D anode and the anode of the control film became larger as current density increased. In addition, the 3D nanostructured anode performed with better rate capability. In general, a reversible Li^+ insertion-extraction in anatase TiO_2 is expressed by the following reaction, associated with a volume change less than 4%:[23]

$$TiO_2 + xLi^+ + xe^- \rightarrow Li_xTiO_2, \ (0 \leq x \geq 1) \quad (4)$$

These two studies in common demonstrated that not only was ALD a viable route for fabricating different 3D

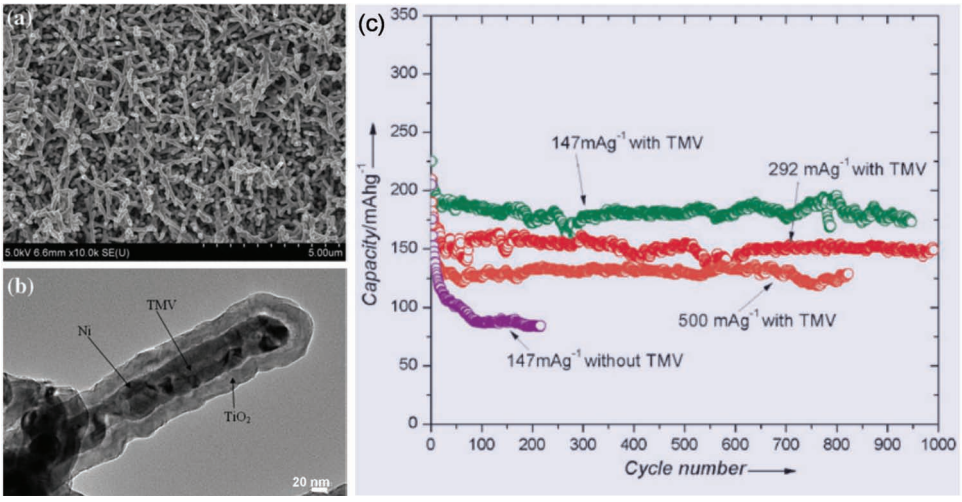

Figure 5. The electrochemical performance of TiO_2-(Ni-TMV) nanocomposites as anode materials for LIBs: (a) low-magnification SEM image for the TiO_2-coated TMV; (b) HR-TEM image for a single composite nanorod including TMV (18 nm), Ni (~20 nm), and TiO_2 (~20 nm); and (c) capacity vs. cycle number for electrodes with and without TMV. Reproduced with permission.[87] Copyright 2010, The Royal Society of Chemistry.

nanostructures but also the nanostructures were superior to the others as LIB anodes. The high performance of the two anodes can be ascribed to the benefits of their unique nanostructures: (1) shortened diffusion paths of lithium ions; (2) facile electronic conduction. In the case of the 3D network of hollow TiO_2 ribbons,[93] lithium ions can easily diffuse from both the outside and the hollow space of the TiO_2 ribbons. In addition, the 3D network helped retain the connection of anode materials and facilitated the conduction of electrons. For TiO_2-(Ni-TMV) core-shell nanocomposites,[87] on the other hand, the robust metalized TMV template contributed to the integrity and low impedance of the resultant TiO_2 structure, thereby enhancing its stability and rate capability.

Besides the above two studies, recently Cheah et al.[77] used ALD-TiO_2 to develop one kind of 3D LIB anodes for microbatteries. Traditionally, the electrodes in LIB microbatteries are 2D planar thin films. To prepare a 3D LIB anode of microbatteries, the researchers deposited a uniform layer of 17 nm TiO_2 (**Figure 6** (b)) on aluminum nanorods[112] (Figure 6(a)). The as-deposited anatase TiO_2 nanostructure as anode showed a dramatic ten-fold increase in total capacity (Figure 6(c)), compared to that of a 17 nm 2D planar TiO_2 film. In this nanostructure, a 4 nm layer of Al_2O_3 (Figure 6(b)) formed between the TiO_2 layer and the Al nanorod, due to the exposure of Al nanorods to air before ALD-TiO_2. Additionally, aluminum nanorods served as current collector. Further, after 50 charge-discharge cycles, the stability of the capacity retention of the 3D nanostructured TiO_2 electrode remained excellent. The reason for the increased capacity of the nanostructured TiO_2 was ascribed to the higher amount of TiO_2 deposited onto the 3D nanostructured Al current collector.

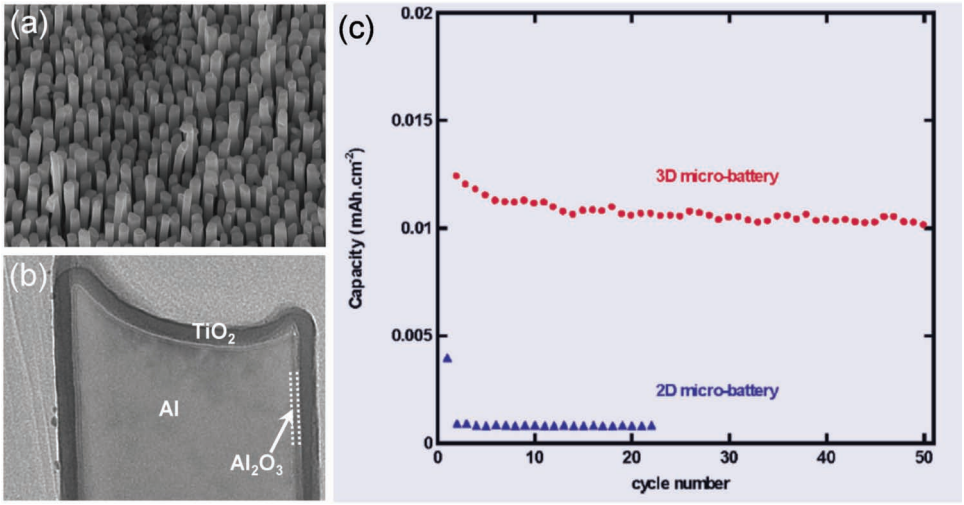

Figure 6. The electrochemical performance of ALD-TiO_2 coated Al nanorods used as anodes of 3D microbatteries: (a) SEM image of Al nanorod arrays; (b) TEM image of an ALD-TiO_2 coated Al nanorod; and (c) normalized capacity (mAh/cm^2 of geometrical surface area) for the 3D microbattery with TiO_2 deposited on an Al nanorod current collector and the 2D electrode with TiO_2 deposited on a flat plate. The galvanostatic cycling current is 0.001 mA. Reproduced with permission.[77] Copyright 2009, American Chemical Society.

In all three studies, the nanostructured anodes were commonly tested with the crystalline anatase TiO_2. Our recent work[113] with amorphous/crystalline SnO_2-GNS nanocomposites revealed that crystallinities of the materials as well as their morphologies significantly influence the performance of LIB anodes. Previously, our studies[91,102–104] disclosed that ALD is capable of directly depositing both amorphous/crystalline TiO_2 and SnO_2 simply by adjusting deposition temperatures. Electrochemical testing[113] showed that the amorphous SnO_2-GNS one, compared to the crystalline SnO_2-GNS and pure GNS one, exhibits much higher specific capacity with extended cycleability (**Figure 7** (a)). In addition, the amorphous SnO_2-GNS anode showed an increased Coulombic efficiency from 97% of the 11th cycle to 99.2% of the 50th cycle and around 100% in subsequent cycles, a value much higher than the that of crystalline SnO_2-GNS electrodes. It is believed that the crystallinities as well as morphologies of the ALD-deposited SnO_2 have affected the resulting electrochemical behaviors. The electrochemical interaction between lithium and SnO_2 can be presented in two steps:

$$SnO_2 + 4Li^+ + 4e^- \rightarrow Sn + 2Li_2O \quad (5)$$

$$Sn + xLi^+ + xe^- \leftrightarrow Li_xSn\ (x \leq 4.4) \quad (6)$$

In the above reactions, SnO_2 electrochemically reacts with Li^+ and thereby leads to the formation of Sn and Li_2O. The Li_2O can serve as a "cushion" to buffer large volume changes during the alloying and de-alloying of Sn with Li. To exploit the underlying mechanisms responsible for the electrochemical behaviors of both amorphous/crystalline SnO_2-GNS, we investigated the changes in the morphology and structure of cycled anodes using SEM and TEM. This revealed that the crystalline SnO_2 underwent severe pulverization, leading to much smaller Sn nanoparticles after 150 charge-discharge cycles. In contrast, the amorphous SnO_2 showed less pulverization and remained almost intact. We ascribed that to its loosened structure and isotropic nature favorable for mitigating volume change and mechanical strain during charge-discharge cycling. For a better understanding, in Figure 7(b) and (c) we schematically illustrate the changes with the amorphous/crystalline SnO_2-GNS anodes during charge-discharge cycles.

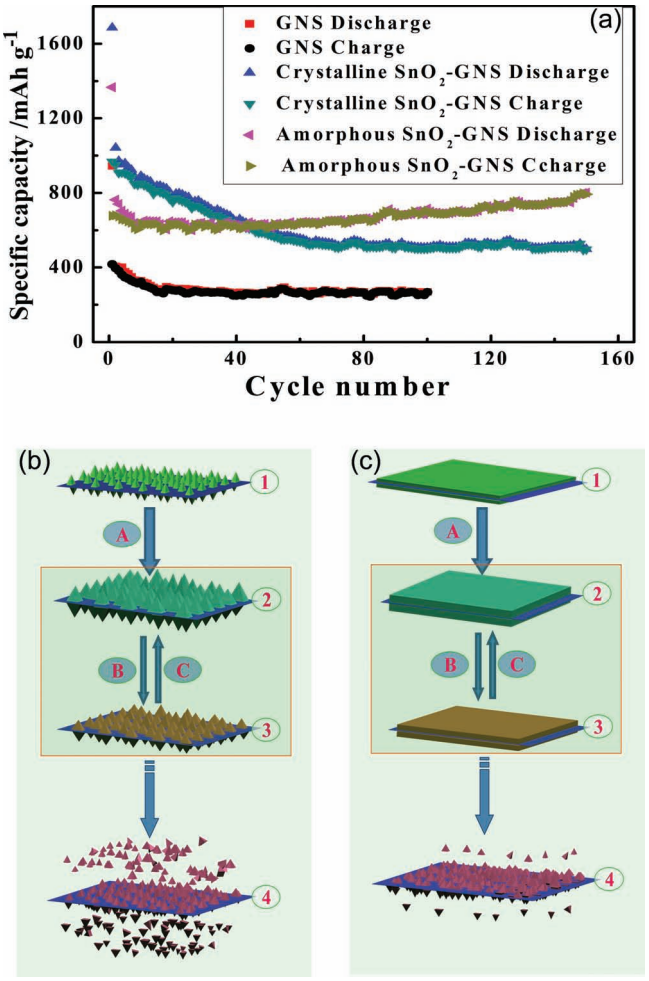

Figure 7. The electrochemical performance of GNS, and ALD-deposited amorphous and crystalline SnO_2-GNS nanocomposites used as anode materials of LIBs: (a) reversible charge-discharge capacity against cycles (the current density of 100 mA/g used for GNS while 400 mA/g used for both amorphous and crystalline SnO_2-GNS nanocomposites in a voltage window of 0.01–3.00 V; and schematically illustration for the morphological evolution of (b) crystalline and (c) amorphous SnO_2-GNS nanocomposite anodes during charge-discharge cycle, i.e., the pristine SnO_2-GNS (1) to transformed to graphene based Li_xSn (2) after the first discharge (A), the alloying (2) and dealloying (3) of Li_xSn happened in the subsequent charge (B) and discharge (C) processes, and then the increased cycling of the composites led to some loss in active materials from graphene matrix, as illustrated by (4). Reproduced with permission.[113]

3.2. Cathodes

Starting from Goodenough's pioneering work,[114,115] many cathode materials of LIBs were developed, including $LiCoO_2$, $LiMnO_2$, $LiMn_2O_4$, $LiNiO_2$, $LiNi_{0.5}Mn_{0.5}O_2$, $LiNi_{1/3}Mn_{1/3}Co_{1/3}O_2$, $LiFePO_4$, and V_2O_5.[3,20,22,24,116] Most are ternary or quaternary elemental compounds. The only one synthesized by ALD to date is V_2O_5 as cathode for microbatteries. As a widely useful metal oxide, V_2O_5 has been prepared in earlier studies by a variety of methods including vapor-phase and solution-based strategies, as reviewed by Wang et al.[19,20] and Beke.[117] V_2O_5 has a layered structure with a theoretical capacity of 442 mAh/g for LIBs.[116] Whittingham[118] first reported the reversible electrochemical lithium intercalation into V_2O_5. Previously, Baba et al.[119] developed a prototype of all-solid-state lithium-ion batteries (ASS-LIBs) using sputtered V_2O_5 as the cathode material and the resultant LIB cell demonstrated excellent electrochemical stability. Using ALD as a design and synthesis route, Badot et al. first successfully deposited amorphous V_2O_5 with vanadyl triisoproproxide (VTOP, $VO(O^iPr)_3$) and water as precursors in the temperature range from 45 to 150 °C.[120,121] They further demonstrated that the annealed (at 400 °C) 700 nm thick V_2O_5 films offered excellent electrochemical stability and cycleability for the insertion-extraction of lithium ions between 3 and 3.8 V.[120] A reversible Li^+ insertion-extraction with anatase V_2O_5 is expressed by the following reaction:[24,120]

$$V_2O_5 + xLi^+ + xe^- \rightarrow Li_xV_2O_5,\ (0 \leq x \leq 1) \quad (7)$$

Later, Baddour-Hadjean et al.[122] used Raman spectroscopy to systematically study the phase changes of an 800 nm thick ALD-V_2O_5 film (annealed at 450 °C) as a cathode of LIBs during the insertion-extraction of lithium ions. With X-ray photoelectron spectroscopy (XPS) and Raman, Le Van et al.[123] further confirmed that the ALD-deposited amorphous vanadium oxide mainly comprised V_2O_5. Interestingly, they reported that the amorphous V_2O_5 is superior as a cathode to crystalline V_2O_5. The amorphous film, with an optimal 200 nm thickness, exhibited higher capacity and better cycleability than its crystalline counterpart, delivering a constant 455 mAh/g at C/10 (one charge-discharge cycle for 10 h).

3.3. Inorganic Solid Electrolytes and Lithium-Containing Films

There are mainly three classes of electrolytes used for LIBs, i.e., liquid, gel or solid polymer, and inorganic solid electrolytes.[5] Liquid electrolytes are the most widely used while inorganic solid electrolytes are still in their infancy.[5] In general, liquid electrolytes contain highly volatile and flammable organic solvents. Consequently, conventional LIBs potentially have safety issues which would become more serious with the increasing size of LIBs for use in EVs.[124] The ultimate solution lies in solvent-free and nonflammable inorganic solid electrolytes.[10,124] They are especially crucial for the development of all-solid-state rechargeable microbatteries that, for example, play a key role in many autonomous devices, such as small medical implants, hearing aids, and integrated lighting solutions.[125] Traditionally, PVD techniques, such as sputtering and evaporation, take the dominant place in manufacturing the components of microbatteries with 2D planar configurations.[30,116] However, the 2D planar thin film batteries suffer from many challenges, as reviewed by Patil et al.[116] To address them in assuring for higher volumetric energy density, 3D architectured battery configurations were proposed, as described in the reviews by Long et al.[126] and Roberts et al.[127] Another alternative configuration has recently proposed by Notten et al.,[128] and the principle is illustrated in **Figure 8**. By depositing different functional layers into the trenches, the surface area is significantly enhanced and thereby the energy density is improved by several orders of magnitudes more than the planar thin film batteries. This has been clearly demonstrated in the aforementioned case of the ALD-TiO_2 conducted by Cheah et al.[77] Due to the line-of-sight drawback of PVD, new techniques are required to satisfy conformal deposition in complex substrates for developing 3D batteries.[127] In this way, ALD is obviously the best choice, as Baggetto et al.[125] pointed out. As we demonstrated in earlier sections, ALD is viable for both the anodes (e.g., ALD-TiO_2[77]) and cathodes (e.g., ALD-V_2O_5[120–123]) of microbatteries. Recent advances also verified that ALD is a key tool for developing inorganic solid electrolytes. **Table 2** summarizes the findings from all the research.

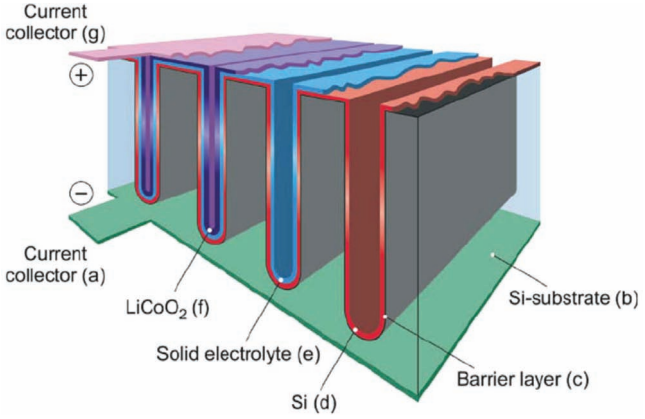

Figure 8. A 3D all-solid-state lithium-ion battery. Reproduced with permission.[128]

Lithium is an important constituent not only in cathode materials but also in inorganic solid electrolytes of LIBs.[29,30] One study[129,130] jointly conducted by researchers from Norway and Finland demonstrated that using ALD they could deposit lithium-containing materials consisting of ternary or quaternary elements, that could serve as inorganic solid electrolytes in ASS-LIBs. Putkonen et al.[129] systematically studied the effects of five different lithium-containing compounds as ALD precursors for depositing lithium-containing thin films, i.e., lithium β-diketonate Li(thd), lithium tert-butoxide Li(O^{t}Bu),

Table 2. ALD-deposited inorganic solid electrolytes/lithium-containing films for LIBs.

Lithium-containing films	ALD subcycles	Precursor A	Precursor B	Growth Temp. [°C]	Substrates	Ref.
$Li_{0.32}La_{0.3}TiO_z$	TiO_2	$TiCl_4$	H_2O	225	Si(111) & soda lime	[129,130]
	La_2O_3	La(thd)$_3$	O_3			
	Li_2O	Li(O^{t}Bu)	H_2O			
Li_2O-Al_2O_3	Al_2O_3	TMA	O_3	225	Si(111) & Teflon	[131]
	Li_2O	Li(O^{t}Bu)	H_2O			
$LiAlSiO_4$	Li_2O	Li(O^{t}Bu)	H_2O	290	Si(400) & Si(004)	[132]
	Al_2O_3	TMA	H_2O			
	SiO_2	TEOS	H_2O			
$Li_2SiO_{2.9}$	$Li_2SiO_{2.9}$	LiN(SiMe$_3$)$_2$	O_3	250	–	[133]
Li_3PO_4	Li_3PO_4	LiN(SiMe$_3$)$_2$	TMPO	225–350	–	
	Li_3PO_4	Li(O^{t}Bu)	TMPO		–	

lithium cyclopentadienyl LiCp, lithium alkyl n-butyllithium n-BuLi, and lithium dicyclohexylamide. It revealed that, combined with suitable oxygen sources such as ozone and water, Li(thd) and Li(O^{t}Bu) are two useful ones. They also demonstrated that the Li(thd)-ozone ALD system incorporated with the La(thd)$_3$-ozone ALD system can produce lithium lanthanate films comprising the tunable constituents of lithium, carbon, lanthanum, and oxygen. In comparison to the Li(thd)-ozone system, the Li(O^{t}Bu)-water system is more beneficial for depositing lithium-containing films, because its carbon content was lower. Later, Aaltonen et al.[130] detailed the deposition of lanthanum titanate and lithium lanthanum titanate (LLT). The latter is considered as a very promising inorganic solid electrolyte, showing very high lithium ionic conductivity at RT.[29–30] Through varying the pulsing ratios of different precursors, the researchers demonstrated that ALD is superior to previous methods such as sputtering and sol-gel for depositing ternary and quaternary systems.[130] In developing ALD-LLT, they combined three subsystems of ALD, i.e., Li(O^{t}Bu)-water, La(thd)$_3$-ozone, and $TiCl_4$-water to deposit LLT at 225 °C. They controlled the composition ratios of the three subsystems (i.e., Li_2O, La_2O_3, and TiO_2) by adjusting their sequence and cycles for each subsystem, termed subcycles. According to the success of each one, TiO_2-La_2O_3-Li_2O was chosen for the ALD-LLT deposition sequence and the LLT deposition was tuned with controlled subcycles using various characterization tools for examination. The as-deposited LLT films was amorphous and deviated from the composition of crystalline LLT. Annealed at 800 °C in oxygen for 3 h, a 100 nm thick $Li_{0.32}La_{0.30}TiO_z$ film matched well with the X-ray diffraction (XRD) patterns of $Li_{0.33}La_{0.557}TiO_3$. However, as Aaltonen et al.[130] remarked, some variance exists in the annealed film with respect to the reported composition of $Li_{0.33}La_{0.557}TiO_3$. In addition, the deposited film contains excess titanium and some XRD peaks were not identified. In subsequent experiments, Aaltonen et al.[131] developed another type of ternary thin films, i.e., Li_2O-Al_2O_3, on Si and Teflon using Li(O^{t}Bu)-water and TMA-O_3 as the ALD precursors, respectively. The films were supposed to be used as a lithium ion conducting barrier layer between an anode and the LLT electrolyte, for LLT is not stable in direct contact with most of anode materials due to the reduction of Ti^{4+} to Ti^{3+}. These as-grown films were amorphous under a deposition temperature of 225 °C. The surface composition of the Li_2O-Al_2O_3 thin films was $Li_{2.2}Al_{1.0}O_z$ determined by XPS while the composition of the dissolved films was $Li_{1.6}$ $Al_{1.0}O_z$ determined by an inductively coupled plasma double focusing sector field mass spectroscopy (ICP-MS).

Other efforts for inorganic solid electrolytes or lithium-containing compounds were also reported at the recent 11th International Conference on ALD (ALD2011, Cambridge, USA). Perng et al.[132] presented their deposition of another solid electrolyte, lithium alumio-silicate ($LiAlSiO_4$). The deposition was performed in a sequence: Li-O, Al-O, and Si-O, using Li(O^{t}Bu), TMA, and tetraethyl orthosilane (TEOS) as metal precursors and water as the oxidant. The individual subcycles affected the metal ratios, and the deposited films were amorphous at 290 °C. Rapid thermal annealing at 900 °C changed the amorphous film into crystalline $LiAlSiO_4$. Hämäläinen et al.[133] described their deposition of lithium silicate and lithium phosphate films. In the former case, they used lithium bis(trimethylsilyl)amide ($LiN(SiMe_3)_2$) and ozone at temperatures ranging from 150 to 400 °C and so generated an amorphous silicate of $Li_2SiO_{2.9}$ at 250 °C with a GPC of 0.8 Å/cycle. They pointed out that temperature affects both GPC and composition. For depositing lithium phosphate, Hämäläinen et al.[133] used trimethylphosphate (TMPO) and either $LiN(SiMe_3)_2$ or Li(O^{t}Bu) as precursors at temperatures ranging from 225 to 350 °C. Crystalline Li_3PO_4 films were obtained in the two processes, containing some traces of carbon and hydrogen.

Recent studies, as reviewed above, demonstrated that ALD exhibits various capabilities in designing LIB components to address the existing issues such as cycling stability, rate capability, and safety. Distinguished from conventional vapor and liquid methods, ALD features its preciseness, low temperature, and conformality in controlling the deposited materials with favorable nanostructures, crystallinity, and compositions. Consequently, ALD makes itself an attractive technique for the development of high performance LIBs.

4. Surface Modification of Battery Electrodes via ALD

Recent progress proved that, besides the value of ALD in directly designing new LIB components, it is an important tool with which we can improve the performance of LIB electrodes via surface coating. LIBs currently suffer from capacity fading during electrochemical cycling and potential safety risks. The major origins of these challenges lie in unwanted side reactions occurring during charge-discharge cycles, causing electrolyte decomposition, SEI formation, and active material dissolution.[12,13,76] To address them and thereby enhance the performance of LIBs, earlier studies demonstrated that surface modification of LIB electrodes is a viable strategy and accordingly it has been investigated extensively. Fu et al[34] and Verma et al.[76] reviewed the previously used modifications for carbon and other anodes. Also, several reviews on modifying cathode materials were conducted by Aurbach et al,[13] Wang et al,[20] Fu et al,[34] Li et al,[35] Yi et al,[36] Myung et al,[37] Chen et al,[38] and Wang et al.[39]

With the progressively accumulating recognition of the value of ALD's characteristics, this technique is receiving much attention as a new strategy to modify LIB electrodes bearing ultrathin coating films. This new strategy was demonstrated to be highly effective in enhancing the electrochemical performance of LIB electrodes. In addition, this approach ensures the formation of a surface coating with high preciseness and flexibility, unobtainable via other conventional methodological counterparts. For example, conventional solution-based techniques require large amount of solvents as well as multiple complex steps, and the resultant coatings are usually in the range of tens of nanometers. In sharp contrast, as a facile vapor technique, ALD dispenses with solvents. The effective coatings generated are several nanometers thick, even down to subnanometers. In comparison to the inability of solution-based methods to directly modify pre-fabricated electrodes, ALD is a practical measure, distinguished from the others as a cost- and time-saving coating technique for LIBs.

4.1. ALD Coatings on Anodes

Anode materials fall into two categories: carbon and non-carbon materials (e.g., metals and metal oxides).[34] Each has some advantages and some disadvantages in LIBs, as we discussed in the section 3.1. In the case of carbon materials, for example, they offer low work potentials but they are prone to induce the decomposition of electrolytes, leading to the formation of a passivation film, i.e., a solid electrolyte interphase, SEI.[12,34,76,134,135] The SEI contains both organic and inorganic products. The former are believed to be the "medium" for transporting lithium cations while the latter ones are considered to be stable against reduction. Thus, the SEI is always bifunctional.[134] However, there is still much unclear in the knowledge of the SEI. Due to the formation of the SEI and the reduction of electrolytes in the first few cycles, irreversible charge loss generally occurs. In addition, the chemistry and properties of the SEI are not fixed and may change during electrochemical cycles.[135] Thus, the properties of SEI influence LIB safety and other aspects of electrochemical performance (e.g., rate capability, cycleability, and self-discharge). To mitigate the energy loss due to the formation of the SEI formation and to enhance LIB safety and overall electrochemical performance, surface coating via solution-based methods previously proved to be effective.

Very strikingly, surface coating via ALD was recently demonstrated to be more beneficial for anode modification. To date, three ALD coatings (including Al_2O_3,[136–143] TiO_2,[144] and TiN[145]) were reported as useful, not just for carbon materials (natural graphite (NG),[136] multiwalled CNTs (MWCNTs)[137]) but also for metal oxides (MoO_3,[138,139] Fe_3O_4,[140] LTO,[141,145] and ZnO[144]) and Si.[142,143] These studies are summarized in **Table 3**, where we also give the ALD parameters and the resulting electrochemical performance. Apparently, ALD-Al_2O_3 is the most widely used coating material.

In these studies, researchers adopted two ALD approaches to modify the electrodes. One was to first coat bare electrode materials via ALD and then fabricate the coated materials into electrodes. This is similar to the process widely adopted by conventional solution-based methods. The second approach was to directly coat the pre-fabricated electrodes made from bare powders. To facilitate identification of these two differently modified electrodes, we name the electrode modified via the former ALD route "E1" and the electrode via the latter route "E2". Usually, in comparison, a control electrode was also prepared using bare electrode materials, called "E0". It is readily evident from Table 3, that the E2 anodes always present the best performance. In other words, the coating approach for the E2 anodes is the most effective one for achieving high electrochemical performance. Apparently, ALD provides a more facile but efficient route to modify anodes that work better.

4.1.1. ALD-Al_2O_3

As the most investigated coating material, ALD-Al_2O_3 is also the first used for electrode modification. The first study of modifying anodes via ALD was conducted by Jung et al. on NG powders.[136] In that work, they noted, using electron dispersive spectrometry (EDS), the uniformity of the direct ALD-Al_2O_3 on a pre-fabricated NG anode along its cross-section (see **Figure 9** (a) and (b)). The resultant E2-NG anode exhibited much better stability than the E0- and E1-NG anode and its capacity was higher than those of the others at the elevated temperature of 50 °C, as illustrated in Figure 9(c). The capacity retention for the E2 and E0 anode was 98% and 26% after 200 charge-discharge cycles, respectively. In contrast, the E1-NG anode behaved even worse than the bare E0-NG anode. It is noteworthy that the effective thin layer of 5-cycle ALD-Al_2O_3 with the E2-NG anode is only around 1 nm. Following the work on NG powders, a recent study[137] also revealed that an ALD-Al_2O_3 coating enhanced the performance of the multi-walled CNTs (MWCNTs) anode. The MWCNTs, grown on a Ti/Ni-coated copper foil via CVD,[137] could be used directly as binder-free anodes. Through directly applying a 10 nm thick layer of ALD-Al_2O_3 on the MWCNTs anode, the resultant E2-MWCNTs anode demonstrated a stable capacity of ~1100 mAh/g in 50 charge-discharge cycles at the current rate of 372 mA/g, i.e., almost three times the theoretical specific capacity of graphite and also much higher than the ~900 mAh/g of the previously reported E0-MWCNTs anode.[146] The capacity of the E2-MWCNTs anode so far supersedes that of any other carbon-nanostructured anodes and any type of oxide-containing anodes. In common, the two groups concluded that the ALD-Al_2O_3 coatings are effective for carbon materials. They believed that a stable "artificial" SEI film of Al_2O_3 protects NG and MWCNTs from undesirable decomposition reactions with electrolytes and has no negative impact on the electron conducting paths between the current collectors and the active materials. Conversely, the worsened performance of the E1-NG powder anode is due to the insulating Al_2O_3 film inhibiting theses electron conduction paths between the current collector and NG powders. To address the effects of ALD-Al_2O_3, recently Leung et al.[147] undertook a numerical modeling. They predicted the decomposition of EC on graphite with or without the ALD-Al_2O_3 coating. The simulations indicated that, without the coating, EC accepts electrons and then decomposes within picoseconds on the surface of a bare lithium metal electrode. In contrast, a layer of ALD-Al_2O_3 coating effectively blocks electron tunneling to the adsorbed EC molecules and thus decreases the decomposition of the electrolyte. The consistency of the simulations supports the experimental claims holding that the ALD-Al_2O_3 coating acted as an "artificial" SEI. In particular, these numerical calculations were also corroborated by microgravimetric measurements.[147]

Compared to traditional carbon materials (e.g., NG) that exhibits little volume change but has a low theoretical specific capacity, non-carbon anode materials display other issues. Many metal oxides and metals (e.g., MoO_3, SnO_2, Fe_3O_4, Sn, and Si), for example, undergo severe pulverization and big volume change during continuous charge-discharge cycles, leading to the failure to contact with current collector and thereby rapid fading of capacity. Recent studies revealed that ALD-Al_2O_3 also efficiently mitigates these problems, and thus improves the performance of the anodes. One typical study was conducted by Riley et al.[138] with MoO_3 nanoparticles. MoO_3 undergoes a 100% volume expansion-contraction during charge-discharge cycles. After coating a pre-fabricated MoO_3 nanoparticle anode via a 4-cycle ALD-Al_2O_3, the resultant E2-MoO_3 anode exhibited no fracturing and showed better cycleability and higher specific capacity than the bare nanoparticle anode (i.e., the E0

Table 3. ALD coatings for surface modification of LIB anodes.

ALD coating materials	ALD coating parameters	Anodes	Performance	Ref.
Al_2O_3	**Precursors**: TMA and H_2O	E0: bare NG powders;	The E2 anode performed better than the other two electrodes in 200 charge-discharge cycles:	[136]
	Temperature: 180 °C	E1: ALD-coated NG powders;	(i) 98% of capacity retention;	
	Thickness: 2–5 cycles; <10 Å	E2: ALD-coated E0 anode.	(ii) nearly 100% of Coulombic efficiency; and	
			(iii) stable performance at elevated temperature (50 °C).	
	Precursors:	E0: MWCNTs directly grown on Cu foils;	The E2 anode performed better than the E0 electrode:	[137]
	TMA and O_2 plasma	E2: ALD-coated E0 anode.	(i) much higher capacity and excellent cycleability;	
	Temperature: 250 °C		(ii) the highest capacity reported for any carbon nanostructures; and	
			(iii) improved mechanical stability.	
	Thickness: ~10 nm			
	Precursors: TMA and H_2O	E0: bare MoO_3 nanoparticles;	The E2 anode performed better than the other two electrodes in 50 charge-discharge cycles:	[138,139]
	Temperature: 180 °C	E1: ALD-coated MoO_3 nanoparticles;	(i) no capacity fading with a stable 900 mAh/g at C/2 rate;	
	Thickness: 4 cycles; <8 Å	E2: ALD-coated E0 anode.	(ii) 97.5% of Coulombic efficiency by the 40^{th} cycle; and	
			(iii) significantly improved adhesion and hardness.	
	Precursors: TMA and H_2O	E0: bare Fe_3O_4 nanocomposites;	The E2 anode performed better than the E0 electrode in durability, rate capability, due to fewer undesirable side reactions.	[140]
	Temperature: 180 °C:	E2: ALD-coated E0 anode.		
	Thickness: 2 cycles; <4 Å			
	Precursors: TMA and H_2O	E0: bare LTO nanoparticles;	The E2 anode performed better than the E0 electrode:	[141]
	Thickness: 0.55–5.5 nm.	E2: ALD-coated E0 anode.	(i) no capacity fading after 100 cycles; and	
			(ii) high Coulombic efficiency with low potential down to 1 mV.	
	Precursors: TMA and H_2O	E0: bare amorphous Si films;	The E2 electrode performed better than the E0 electrode:	[142]
	Thickness: ~5 nm.	E2: ALD-coated E0 Si films.	(i) improved Coulombic efficiency;	
			(ii) less cracking; and	
			(iii) a thinner SEI layer.	
	Precursors: TMA and H_2O	E0-1: bare Si films;	The E2 anode performed better than both the E0-1 and E0-2 electrode:	[143]
	Temperature: 250 °C:	E0-2: bare Si columns;	(i) improved capacity retention;	
	Thickness: 2 cycles; <2 nm	E2: ALD-coated E0-2 anode.	(ii) improved Coulombic efficiency; and	
			(iii) less cracking.	
TiO_2	**Precursors**: $TiCl_4$ and H_2O	E0: bare ZnO nanorods;	The E2 anode performed better than the E0 electrode:	[144]
	Temperature: 500 °C:	E2: ALD-coated E0 anode.	(i) improved capacity and retention;	
	Thickness: 200 cycles; ~11 nm		(ii) improved stability; and	
			(iii) fewer undesirable reactions.	
TiN	**Precursors**: $TiCl_4$ and NH_3	E0: bare LTO nanoparticles;	The E1 anode performed better than the E0 electrode:	[145]
	Temperature: 500 °C:	E1: ALD-coated LTO nanoparticles.	(i) no capacity fading;	
	Thickness: 200 cycles; ~5.8 nm		(ii) excellent rate capability; and	
			(iii) better conductivity.	

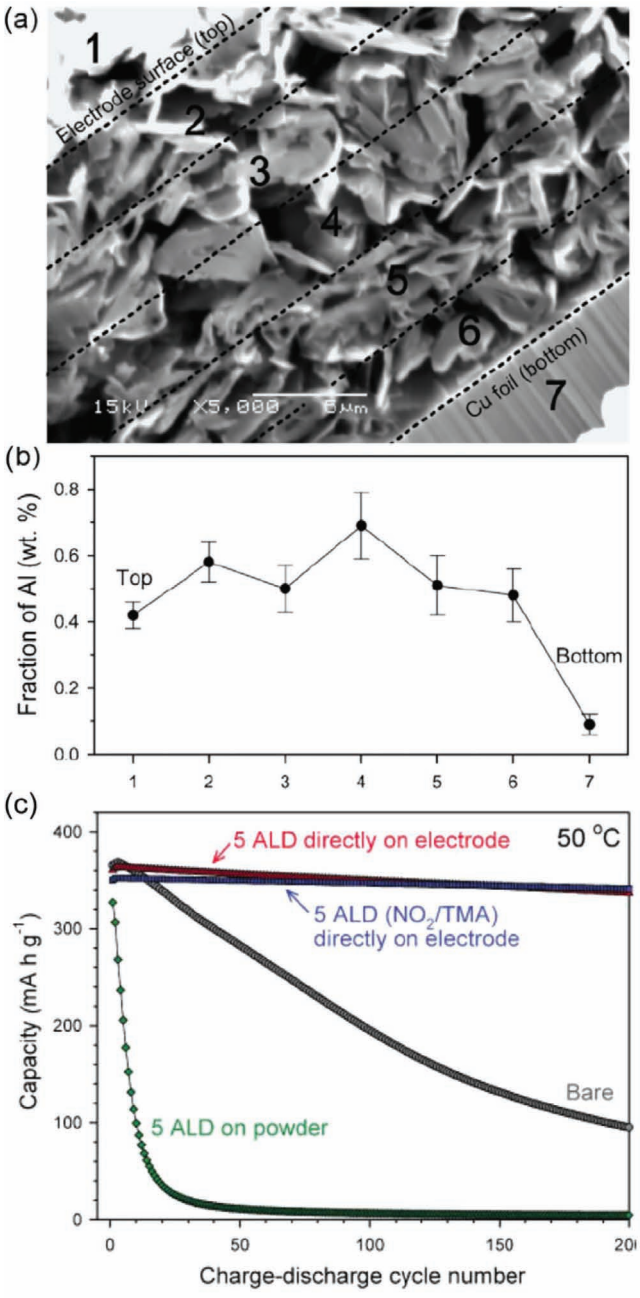

Figure 9. SEM and EDS analyses of ALD-Al_2O_3 coated electrodes: (a) FE-SEM cross-sectional image of NG composite electrode coated with 5 cycles of ALD-Al_2O_3 (numbers indicate regions in which Al was analyzed with EDS); (b) weight fraction of Al as a function of depth; and (c) electrochemical performance of different anodes at 50 °C. Reproduced with permission.[136]

anode). However, the E1-MoO_3 nanoparticle anode displayed worsened electrochemical performance. Riley et al.[138] believed that, besides its protective role as a artificial SEI layer discussed above, the ALD-Al_2O_3 coating on the E2-MoO_3 anode has another function, i.e., strengthening its mechanical stability, as illustrated by **Figure 10**. The white circles represent MoO_3 nanoparticles, the smaller black circles indicate the conductive additives, and the grey surfaces signify the ALD-Al_2O_3 coatings. The bare E0 anode fractured during charge-discharge cycles, due to large volume changes of the MoO_3 nanoparticles. In turn, the fracturing caused the failure of the electrical contact and subsequently the reduced amount of available active materials, therefore resulting in a fading capacity with the increasing number of electrochemical testing cycles (Figure 10(a)). On the other hand, the ALD-Al_2O_3 coatings on the MoO_3 nanoparticles of the E1 anode worsened electronic conductivity between the nanoparticles and the current collector, thereby engendering a decreased capacity of the fabricated E1 anode (Figure 10(b)). In contrast, a direct ALD-Al_2O_3 coating on the E2 anode favorably "knitted" the MoO_3 nanoparticles together and helped retain electric conductivity and mechanical integrity (Figure 10(c)). The layer might work partially even after some cracking had appeared in the MoO_3 nanoparticles. These authors confirmed their postulation on the mechanical role of the ALD-Al_2O_3 coatings in another experiment.[139] Using nanoindentation and nanoscratching, Riley et al.[139] revealed that the adhesion of the E2-MoO_3 nanoparticle anode to the current collector was even more than doubled while the electrode's hardness was increased by close to 50%. Similarly, Dafinone et al.[148] demonstrated in abrasion tests that a 1 nm thick (10 ALD-cycles) ALD-Al_2O_3 coating dramatically improves the mechanical durability of the TiO_2-SiO_2 nanoparticle layer-by-layer films on both inorganic and organic substrates. Similarly, the effectiveness of the ALD-Al_2O_3 coating was demonstrated with another metal oxide, an Fe_3O_4 nanostructured material, whose E2 anode showed improved electrochemical performance.[140]

Interestingly, ALD-Al_2O_3 coatings were recently used for Si anodes. Si is a very promising anode material with a high theoretic capacity up to 4000 mAh/g.[6,10] However, it undergoes a dramatic volume expansion (>300%) during lithiation, making its usage impractical in LIBs. Two recent studies[142,143] both demonstrated that putting a layer of ALD-Al_2O_3 coating on Si anode, i.e., generating E2-Si anodes, has greatly improved the performance of the resultant E2 Si anodes. With a 5 nm ALD-Al_2O_3 coating, Xiao et al.[142] noted that the E2-Si anode has less micro-cracks than do bare E0-Si films (**Figure 11** (a) and (b)), confirming that the ALD coating prevents the mechanical degradation of the Si films. He et al.[143] observed similar phenomena on Si columns. With a coating of around 2 nm ALD-Al_2O_3 films, the resultant E2-Si column electrode displayed enhanced capacity retention and Coulombic efficiency (Figure 11(c) and (d)). To clarify the intriguing roles of ALD-Al_2O_3 on Si anodes, Xiao et al.[142] characterized the SEI thickness and compositions with those of the bare E0- and E2-Si anode using time-of-flight secondary ion mass spectrometry (TOF-SIMS). Their results disclosed that the SEI thickness with the E0-Si anode is around 20–30 nm while only a few nanometers for the E2-Si anode. Their characterization of the SEIs' compositions showed LiF and Li_2CO_3 commonly existing in the SEI layers of the two anodes, but, of the two anodes, the E2-Si one contained much less Li_2CO_3. They ascribed this to the insulating Al_2O_3 coating preventing electrons from reaching the anode surface to engender the decomposition of the electrolyte. The XPS results disclosed that the SEI on the E2-Si anode has $LiAlO_2$ and AlF_3. $LiAlO_2$ was on the top surface and it helps reduce the energy barriers against the insertion of lithium ions, thus enhancing the kinetics of Li^+ transfer.

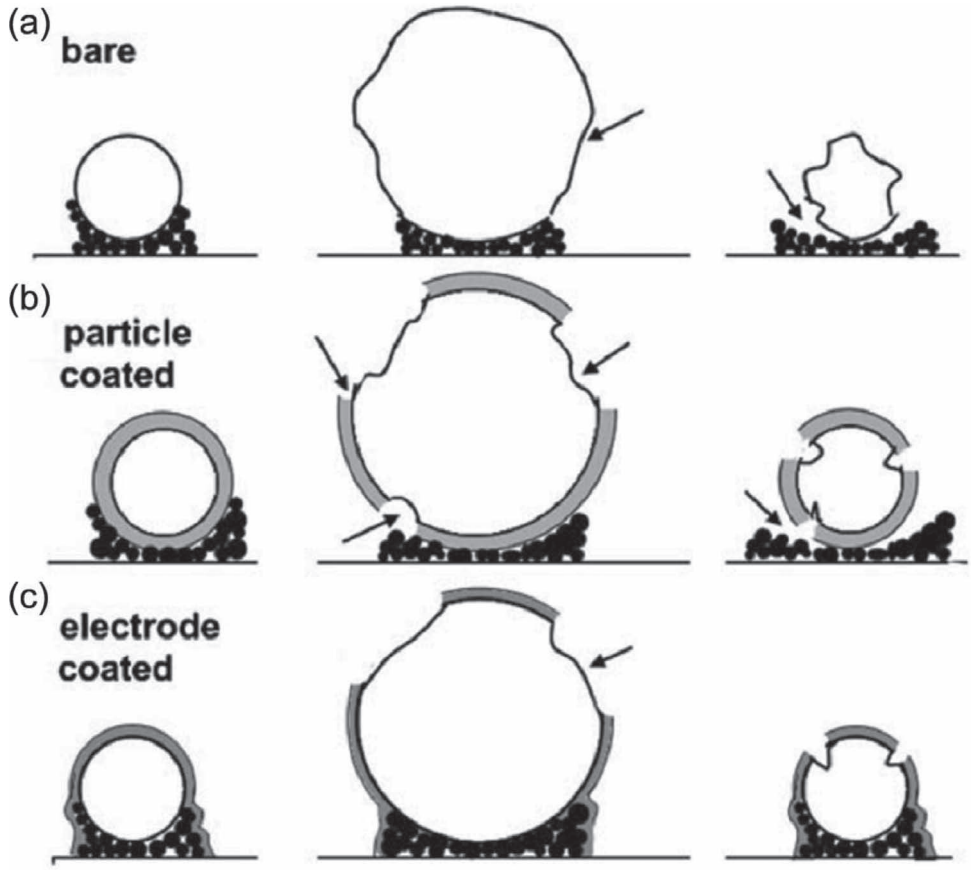

Figure 10. Schematic representation of the effects of volume expansion upon (a) bare particles, (b) ALD coated nano-MoO_3 particles, and (c) particles from an ALD coated porous anode. Reproduced with permission.[138]

More direct evidence for the roles of ALD-Al_2O_3 coating on metal anodes was recently reported by Liu et al.[149] Using an in situ high resolution transmission electron microscopy (HR-TEM), they investigated the changes with an Al_2O_3-coated Al nanowire anode during charge-discharge cycles (**Figure 12**). As a potential anode material, the metal Al has a relatively high theoretical capacity of ~993 mAh/g and a volume expansion around 97%. The in situ HR-TEM uncovered a series of facts, powerfully addressing the effects of the Al_2O_3 coating layer. During lithiation-delithiation cycles, the pristine Al nanowire became curved (Figure 12(b)), reflecting volume expansion-contraction. In this process, nanovoids formed, increasing in number and size. Consequently, the Al nanowire fragmented into many isolated nanoparticles (due to pulverization of the metal electrode, Figure 12(c)) enclosed by a glass tube. The pristine amorphous Al_2O_3 layer of 4–5 nm (Figure 12 (d)) increased to about 6 nm (Figure 12 (e)). This surface layer served as a closed tube, confining the pulverized Al nanoparticles and thereby preventing them from losing contact with the current collector. In particular, the thickness of the surface layer remained unaltered after the first lithiation, but changed from the initial Al_2O_3 coating into the stable Li-Al-O glass, a good solid electrolyte with a lithium ion conductivity at about 10^{-6} S/cm. These researchers also discovered that the surface Al_2O_3 layer had evolved into the Li-Al-O solid electrolyte before the lithiation of the inner Al core, and that the so-formed Li-Al-O did not change in following lithiation-delithiation cycles. However, these researchers did not use liquid electrolytes, so that their results are only partially useful for considering some potential roles of ALD-Al_2O_3 coatings. Further studies are needed to unearth more details about ALD-Al_2O_3 coatings.

Besides the ALD-Al_2O_3 coatings on carbon materials, binary metal oxides, and metals, there is also another report by Ahn and Xiao on LTO nanoparticles,[141] disclosed another functional role. As we stated in the section of 3.1, LTO is a promising anode material to replace graphite, due to several advantages: zero strain, no formation of SEI and lithium metal plating, and stability at high temperatures (75–80 °C) during charge-discharge cycles. However, its high working potential (around 1.55 V vs. Li^+/Li) is the limiting factor for its usage in high energy density devices. Ahn and Xiao[141] found that a layer of ALD-Al_2O_3 coating (<5 nm) on the LTO nanoparticles extend the working potential to 1 mV. In addition, the ALD-Al_2O_3 coating markedly improved cycling stability (no capacity degradation in 100 cycles) and Coulombic efficiency. They believed that the ALD-Al_2O_3 coating stabilized the LTO structure at low potentials (<1 V) and suppressed the formation of SEI.

From the findings of these studies we discussed,[136–143,147–149] it is easy to discern that the multifunctional roles of ALD-Al_2O_3 coatings on the various anodes are, including (1) strengthening the mechanical integrity of the anodes; (2) acting as a kinetic barrier against electron transfer to the organic carbonate molecules of the electrolytes, so protecting the anodes from

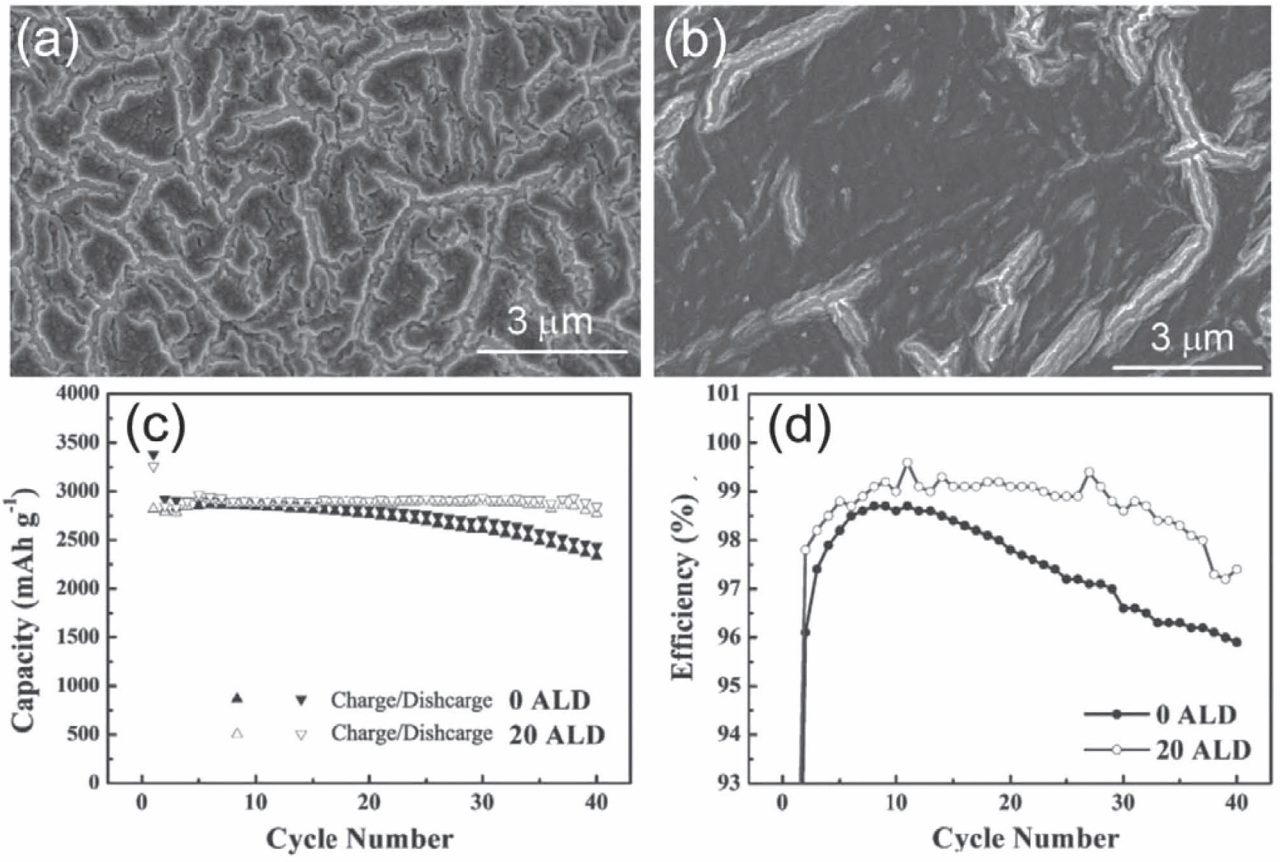

Figure 11. SEM observation on Si anodes: (a) cycled Si; (b) cycled ALD-Al_2O_3 coated Si. Reproduced with permission.[142] Comparison of pristine and ALD-Al_2O_3 coated patterned Si electrodes in the range of 0.005 to 2 V: (c) capacity; (d) Coulombic efficiency. Reproduced with permission.[143]

undesirable reactions; (3) forming an artificial SEI which is chemically stable but highly conductive for lithium ions; and, (4) serving as a stabilizer at low work potential, especially for LTO. Even so, we still lack the knowledge needed for exactly understanding the roles played by the ALD-Al_2O_3 coatings, and undoubtedly, more extensive investigation is needed in future.

4.1.2. ALD-TiO_2 and ALD-TiN

In addition to the Al_2O_3 coatings, TiO_2 is another metal oxide coating reported for surface modification of anodes via ALD. An ALD-TiO_2 process was used to coat a ZnO nanorod anode.[144] ZnO as an alternative anode material of LIBs has a high theoretical capacity but a high volume expansion. Severe morphology and volume changes were previously observed in charge-discharge cycles and these deteriorated the performance of ZnO as anodes.[150,151] With a 200-cycle ALD-TiO_2 (~11 nm) coating, a coated ZnO nanorod anode (i.e. an E2 anode) exhibited an improved reversible capacity, accounting for 447 mAh/g compared to 358 mAh/g for the uncoated ZnO nanorod anode (i.e., an E0 anode).[144] In addition, the ALD-TiO_2 coating helped maintain the coated ZnO nanorods perpendicular to the substrate while the bare ZnO nanorods only survived for 30 cycles. Besides sustaining the mechanical integrity of ZnO nanorods, it was believed that the ALD-TiO_2 acts as an "artificial" SEI reducing the degree of reactions between ZnO and the electrolyte, and thereby helping improve the stability of charge-discharge cycles.

One non-oxide ALD coating was recently reported in literature, i.e., an ALD-TiN coating. Snyder et al.[145] applied an ALD-TiN thin film on LTO powders. LTO is essentially insulating, leading to capacity fading with increasing numbers of charge-discharge cycles. Many strategies have been used to improve the electronic conductivity of LTO, and surface modification was applied with many coating materials (e.g., Ag, carbon, SnO_2, TiN, as well as organic compounds).[152] Of them, TiN afforded a series of beneficial factors, such as its hard, refractory, and metallic properties. Using urea as nitrogen source, for example, researchers recently coated LTO particles with TiN via heat treatment.[153] The modified LTO particles displayed improved rate capability and cycleability. Using the ALD technique, Snyder et al.[145] coated LTO nanoparticles of 25 nm with ALD-TiN at 500 °C. A 200-cycle coating led to an average thickness of ~5.8 nm, accounting for an approximate GPC of 0.3 Å/cycle. A such ALD-coated LTO nanoparticle anode (i.e., an E1 anode) showed a remarkably improved performance. The ALD-coated LTO anode nearly maintained its specific capacity at the theoretical value of 167.5 mAh/g over numerous charge-discharge cycles at different charge rates. In contrast, the uncoated LTO anode displayed a drastic decrease in specific capacity with increased charge rates and reached its lowest specific capacity of 60 mAh/g after the third charge at C/5. The researchers believed

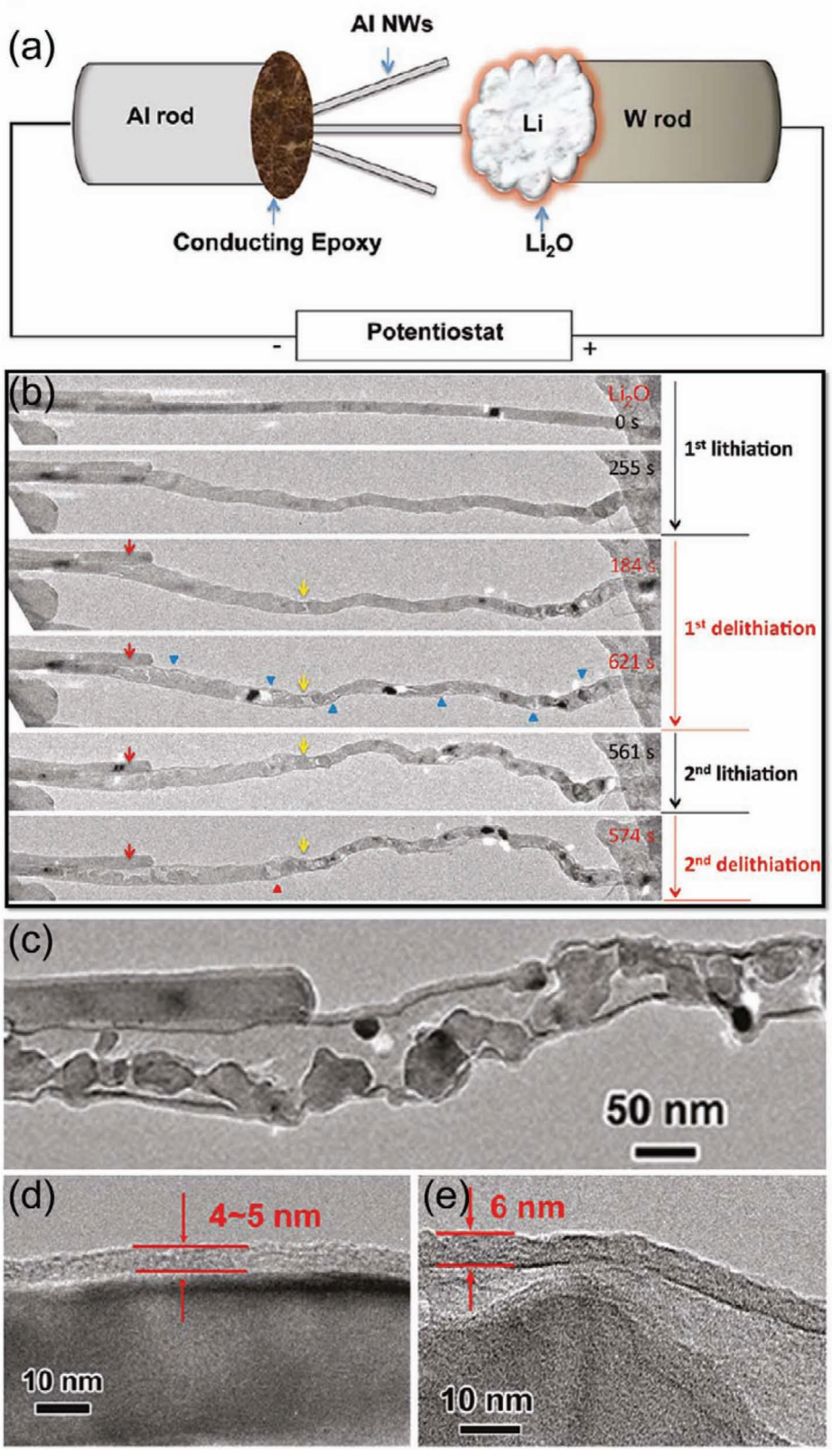

Figure 12. In situ HR-TEM observation on the structural changes in an Al_2O_3-covered Al nanowire during electrochemical cycling: (a) schematic illustration of the in situ experimental setup; (b) morphological evolution on cycling of a single Al nanowire covered by a Al_2O_3 layer; (c) TEM image of a local area of the Al nanowire after the fourth cycle; and TEM images of the surface layers of (d) the pristine Al nanowire and (e) the nanowire after the fourth cycle. Reproduced with permission.[149] Copyright 2011, American Chemical Society.

that the ALD-TiN had the following favorable effects on the LTO nanoparticles: (1) the removal of electrically non-conducting carbonate species during ALD; (2) the improved electrical contact of LTO particles due to the presence of the TiN thin film.

4.2. ALD Coatings on Cathodes

The cathode active materials in LIBs are largely responsible for many factors such as toxicity, thermal stability, safety, and energy and power density. The direct contact of cathode materials with liquid electrolytes entails many detrimental side reactions occurring slowly at ambient temperature, resulting in the slow degradation of electrode materials and ultimately, the defective battery performance. Researchers tried substituting partially active elements with alkaline metals and Al to stabilize electrode structures and thereby to enhance cycleability and thermal stability.[12] However, such substitution often lowered capacity and Li^+ diffusion, since the substituents mainly are electrochemically inactive ingredients. Alternatively, in comparison, surface coating is much simpler and also more beneficial, in that it has also no influence on the amount of electrochemically active elements of cathodes that, therefore, do not incur any loss in their capacity. Since Amatucci and Tarascon patented the surface modification of cathodes in 1998,[154] many research groups have demonstrated the viability of nanoscale oxide coatings in significantly improving reversibility and reliability in the high voltage region (above 4.3 V vs. Li/Li^+), as reviewed in the literature.[34–38] Chen et al. recently categorized the effects of various surface coatings into four classes:[38] (1) higher ionic conductivity; (2) improved performance due to the cathode's modified surface chemistry; (3) HF scavengers that suppress metal dissolution from cathode materials; and, (4) physically protective barriers that impede side reactions between cathode materials and electrolytes.

Parallel to the studies of using ALD to modify anodes, there was a rise in the number of reports on cathode materials. Three kinds of cathode materials have been modified by ALD coatings, including $LiCoO_2$,[155–157] $LiNi_{1/3}Mn_{1/3}Co_{1/3}O_2$,[158] and $LiMn_2O_4$.[159] The high effectiveness of ALD-Al_2O_3 was again demonstrated in enhancing the electrochemical performance of the cathode materials. A new coating material, ALD-ZnO, was also considered but had no evident favorable effect on $LiCoO_2$. **Table 4** summarizes these studies. Similar to its applications in

Table 4. ALD coatings for surface modification of LIB cathodes.

ALD coating materials	ALD coating parameters	Cathodes	Electrochemical performance	Ref.
Al_2O_3	**Precursors**: TMA and H_2O	E0: bare $LiCoO_2$ micropowders;	The E1 and E2 cathode exhibited comparable capacity and stability, and both performed better than the E0 cathode in capacity, and capacity retention.	[155]
	Temperature: 180 °C	E1: ALD-coated $LiCoO_2$ powders;		
	Thickness: 2–5 cycles; <10 Å	E2: ALD-coated E0 cathode.		
	Precursors: TMA and H_2O	E0: bare $LiCoO_2$ micropowders; E2: ALD-coated E0 cathode.	The E2 cathode showed improved cycleability.	[156]
	Temperature: 120 °C			
	Thickness: 10–500 cycles; <150 nm			
	Precursors: TMA and H_2O	E0-1: bare $LiCoO_2$ micropowders;	The E2 cathode performed much better than the two E0 cathodes:	[157]
	Temperature: 180 °C	E0-2: bare $LiCoO_2$ nanoparticles;	(i) dramatically improved capacity retention; and,	
	Thickness: 2–6 cycles; <11 Å	E2: ALD-coated E0-2 cathode.	(ii) 250% improvement in reversible capacity at the high rate of 7.8 C.	
	Precursors: TMA and H_2O	E0: bare $LiNi_{1/3}Mn_{1/3}Co_{1/3}O_2$ nanoparticles;	The E1 cathode performed better than the E0 cathode when the coating was less than 6 cycles (12 Å):	[158]
	Temperature: 180 °C	E1: ALD-coated $LiNi_{1/3}Mn_{1/3}Co_{1/3}O_2$ nanoparticles.	(i) improved stability; and,	
	Thickness: 2–10 cycles; <22 Å		(ii) enhanced capacity retention.	
	Precursors: TMA and H_2O	E0: bare $LiMn_2O_4$ micropowder;	The E1 cathode performed better than the E0 cathode with improved cycleability.	[159]
	Temperature: 120 °C	E2: ALD-coated E0 cathode.		
	Thickness: 10–20 cycles; <4 nm			
ZnO	**Precursors**: $Zn(CH_2CH_3)_2$ and H_2O	E0: bare $LiCoO_2$ micropowders;	The ALD-ZnO coating had no evident improvement on electrochemical performance, due to its instability.	[155]
	Temperature: 180 °C:	E1: ALD-coated $LiCoO_2$ micropowders.		
	Thickness: 4 cycles; <8 nm			

modifying anodes, the beneficial effects of ALD-Al_2O_3 on the cathodes are evident in processing costs and time.

4.2.1. ALD-Al_2O_3

Of cathode materials, $LiCoO_2$ is one widely used in commercial LIBs. However, it undergoes structural degradation at high cut-off charge voltage (above 4.1 V) during charge-discharge cycles. Earlier studies demonstrated that various surface coatings enhanced the electrochemical performance of $LiCoO_2$, such as carbon, Li_2CO_3, $LiMn_2O_4$, $Li_4Ti_5O_{12}$, MgO, Al_2O_3, $AlPO_4$, SiO_2, TiO_2, ZrO_2, SnO_2, and La_2O_3.[35,160–165] The main coating techniques previously employed were solution-based ones.[37] Jung et al. first reported using ALD as a technique for surface coating of cathodes.[155] They employed ALD-Al_2O_3 to coat $LiCoO_2$ micropowders of 7–10 μm, finding that the resultant E1-$LiCoO_2$ micropowder cathode has a dramatically improved capacity retention during charge-discharge cycles regardless of the thickness of the ALD coatings. In comparison to a 45% capacity retention for the E0-$LiCoO_2$ cathode, the E1-$LiCoO_2$ cathode exhibited a capacity retention of 89% after 120 charge-discharge cycles in the 3.3–4.5 V (vs. Li/Li^+) range (**Figure 13**). Among three ALD-cycles (2, 6, and 10 cycles), the 2-cycle ALD-Al_2O_3 coating (~3 to 4 Å thick) produced an initial capacity comparable to that of the E0-$LiCoO_2$ cathode. In comparison, the initial decline in capacity with Al_2O_3 coatings increased from 6 to 10 ALD-cycles, probably due to the restricted electron transport and the slower Li^+ diffusion kinetics in the ALD-Al_2O_3 layers. Jung et al.[155] also observed that the presence of the ALD-Al_2O_3 coatings greatly stabilized the interface between the electrolyte and the $LiCoO_2$ cathode. As an alternative route, the direct coating of 2-cycle ALD-Al_2O_3 on a pre-fabricated $LiCoO_2$ composite cathode, i.e., the E2-$LiCoO_2$ cathode, was investigated. It was demonstrated that the performance of this E2-$LiCoO_2$ cathode was comparable to that of the E1-$LiCoO_2$ cathode. However, the E2 cathode offers several additional advantages over the E1 cathode: (1) less coating materials, accounting for a 3–4 Å ALD coating with respect to a 100–1000 Å thick film by wet chemical methods; (2) a coating free of solvents; (3) a facile but high efficient route. Another research team used the ALD-coating route for fabricating E2 cathodes with another kind of $LiCoO_2$ micropowders.[156] Their study supported that, compared to an E0-$LiCoO_2$ cathode, thin Al_2O_3 coatings of less than 50 ALD-cycles improved capacity and cycleability, while thicker ones from more than 50 ALD-cycles reduced capacity. Using one kind of nanosized $LiCoO_2$ (400 nm) as cathode material, Scott et al.[157] more recently confirmed that a direct coating of 2-cycle ALD-Al_2O_3 on a prefabricated cathode (i.e., an E2 cathode) greatly improved capacity retention in 200 charge-discharge cycles at a high current density 1400 mA/g (7.8 C) (**Figure 14**), so accounting for a 250% improvement in reversible capacity compared to the E0-$LiCoO_2$ nanoparticle cathode. Conversely, a 6-cycle ALD-Al_2O_3 coating engendered many detrimental effects such as the poor conductivity of lithium ions and a larger overpotential. Considering that the difference in thickness between 2 and 6 ALD cycles is between 2.2 and 11 Å, these findings demonstrated the need for controlling ultrathin coatings at the nanoscale. Considering the roles of the ALD-Al_2O_3 coatings in these studies, it was believed that they might have helped suppress structural instabilities during lithium insertion-extraction, acted as a solid electrolyte, prevented the direct contact between the cathode surface and the electrolyte, and served as a scavenger for HF resulting from the reaction of trace amounts of water with $LiPF_6$ in the electrolyte. The results of XPS supported the last role, showing that some AlF_3 formed on the coated powders.[155]

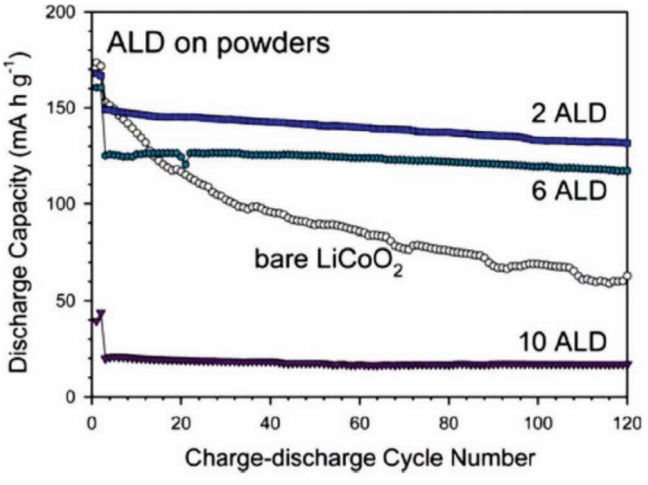

Figure 13. Charge-discharge cycle performance of electrodes fabricated from bare $LiCoO_2$ powders and the ALD-Al_2O_3 coated $LiCoO_2$ powders using 2, 6, and 10 ALD cycles. Reproduced with permission.[155] Copyright 2010, The Electrochemical Society.

$LiNi_{1/3}Mn_{1/3}Co_{1/3}O_2$ is a replacement material for $LiCoO_2$, which was first proposed by Ohzuku and Makimura.[166] It offers a high discharge capacity and reduces the cost and toxicity of Co.[167,168] Unfortunately, $LiNi_{1/3}Mn_{1/3}Co_{1/3}O_2$ has poor rate capability and experiences considerable capacity loss at high current density. To improve its electrochemical characteristics, different surface coatings (e.g., Y_2O_3,[167] AlF_3,[168] and Al_2O_3[169,170]) deposited via solution-based methods were found to engender much improvement. Recently, Riley et al.[158] reported the improvement in the reversibility of ALD-Al_2O_3 coated $LiNi_{1/3}Mn_{1/3}Co_{1/3}O_2$ nanoparticles (200-400 nm) (i.e., the E1 cathodes), compared to an uncoated one. They also found that Al_2O_3 coatings of 2-6 ALD-cycles are beneficial to the nanoparticles' electrochemical performance, a coating of more than 10 ALD-cycles (~2 nm) is detrimental. An ALD coating of less than 6 cycles helped $LiNi_{1/3}Mn_{1/3}Co_{1/3}O_2$ nanoparticles maintain 80% initial capacity after 110 cycles. On the contrary, a coating thicker than ~1.2 nm (corresponding to 6 ALD cycles) severely hindered the electrochemical stability of the nanoparticles. The roots may lie in the reduced kinetics of ion and electron transport with the increased thickness of the coatings. Additionally, a thick coating tends to physically isolate individual particles from direct contact with conductive additives such as acetylene black. In contrast to the coatings of several or even several tens of nanometers by wet chemical methods, the ALD coatings are much thinner and ALD is also more facile in operation. Hence, compared to the coatings prepared via solution-based methods, a comparable effectiveness with the much thinner ALD-coatings may account for the difference in the coating quality and properties.

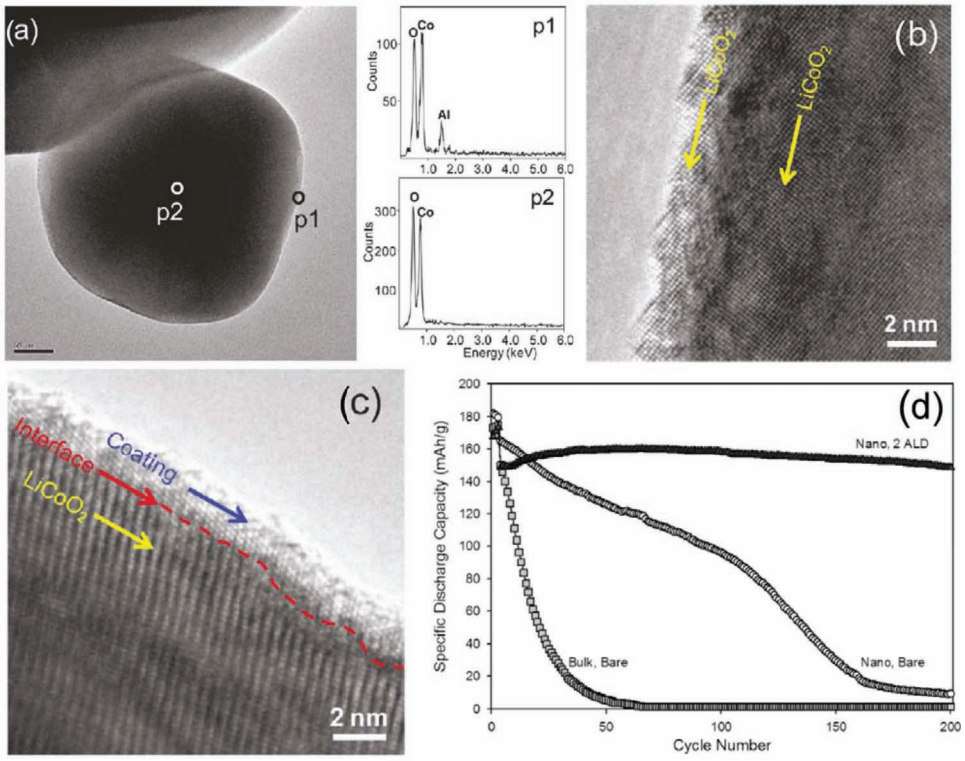

Figure 14. The effects of the ALD-Al_2O_3 coatings on the electrochemical performance of nano-$LiCoO_2$ particles: (a) 2-cycle ALD-Al_2O_3 coated nanoparticles (left), showing the presence of Al by XDS spectrum (right); (b) HR-TEM image for a bare nanoparticle; (c) HR-TEM image for a 2-cycle ALD-Al_2O_3 coated nanoparticle; and (d) the cycleability of different cathodes fabricated by the bare bulk-$LiCoO_2$, bare nano-$LiCoO_2$, and 2-cycle ALD-Al_2O_3 coated nano-$LiCoO_2$. Reproduced with permission.[157] Copyright 2011, American Chemical Society.

The spinel $LiMn_2O_4$ is another potential replacement for $LiCoO_2$ with the merits of low cost and high safety. However, $LiMn_2O_4$ is easy to degrade in capacity, especially at elevated temperature (>55 °C), due to its structural instability, the decomposition of the electrolyte, the dissolution of manganese ions, and Jahn-Teller distortion.[36] Surface coatings via solution-based methods (e.g., metals such as Co[171] and Au,[172] metal oxides such as Al_2O_3,[173] TiO_2,[174,175] ZnO,[176] and Cr_2O_3,[177] and others[36]) can enhance the electrochemical performance of $LiMn_2O_4$. Using ALD-Al_2O_3, Guan et al.[159] recently demonstrated that the coating via ALD is a facile but highly efficient route. With one kind of commercial $LiMn_2O_4$ micropowders (1–8 μm), two kinds of cathodes were comparatively investigated. It was found that two E2-$LiMn_2O_4$ cathodes exhibits improved capacity retention and higher capacities than that of a bare E0-$LiMn_2O_4$ cathode in a long-time cycling in a potential range of -0.3-0.8 V vs. Ag/Ag^+ (**Figure 15**). The discharge capacity of the bare E0 cathode fell continuously from 52.6 to 32.1 mAh/g over 100 cycles, while the two E2 cathodes started from lower capacities and recovered to higher ones with extended charge-discharge cycles. The low initial capacities might be caused by the insulating Al_2O_3 coatings. In comparison, the E2 cathode with a thinner coating of 10 ALD-cycles showed higher capacities and better cycleability than the E2 cathode with a thicker coating of 20 ALD-cycles, probably due to less surface resistance. Thus, there is an optimal cycling number of ALD-Al_2O_3 for the best electrochemical performance. Furthermore, Guan et al[159] confirmed that the ALD-Al_2O_3 coatings were partially dissolved in the electrolyte, for no Al element was detected by XPS on a 4-cycle ALD-Al_2O_3 coated cathode after 100 charge-discharge cycles. They thought that the dissolution of manganese was the reason of the capacity fading. Due to the protective ALD-Al_2O_3 coatings, however, the E2 cathodes delivered higher capacities than the bare cathode after 100 cycles. In addition, Guan et al.[159] pointed out that, assuming a growth rate of 2.0 Å/cycle for ALD-Al_2O_3, the ALD-Al_2O_3 coatings (<4 nm) are much thinner than the ones (50–100 nm in thickness) previously prepared by wet chemical methods, but they produced a comparable electrochemical performance.

Certainly, all these studies on the three cathode materials demonstrated in common that ALD-Al_2O_3 provides an efficient route for high-performance cathodes. The roles played by the ALD-Al_2O_3 coatings are consistent to the four classes summarized by Chen et al.[38] The exact mechanisms involved need further investigation in future.

4.2.2. ALD-ZnO

Besides the ALD-Al_2O_3 coating, Jung et al. investigated an ALD-ZnO coating to modify $LiCoO_2$.[155] Unfortunately, there was no evident improvement observed with the cycling performance of a resultant E1-$LiCoO_2$ cathode. The reason might lie in the instability of the ALD-ZnO layers on the $LiCoO_2$ powders, as suggested by XPS results.

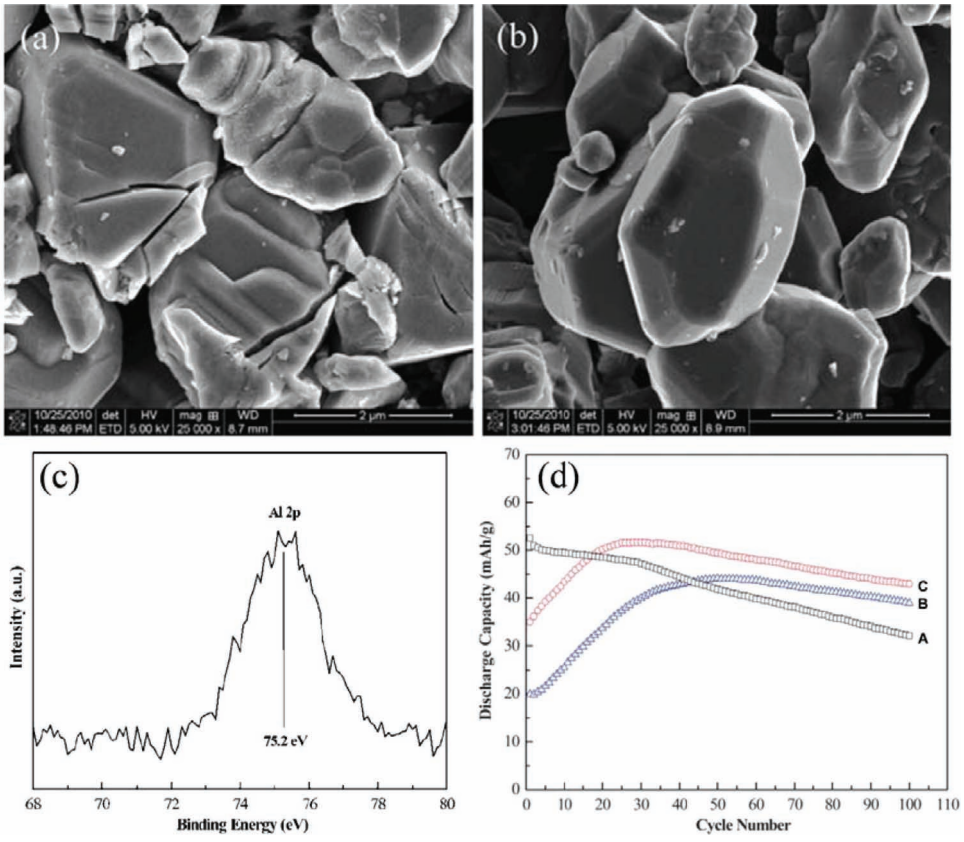

Figure 15. The effects of the ALD-Al_2O_3 coatings on the electrochemical performance of $LiMn_2O_4$ cathodes: (a) the bare $LiMn_2O_4$ micropowders; (b) the 20-cycle ALD-Al_2O_3 coated $LiMn_2O_4$ micropowders; (c) XPS spectrum from $LiMn_2O_4$ cathode coated by 4-cycle Al_2O_3; and (d) cycling performance of (A) the bare $LiMn_2O_4$ cathode, and the cathodes coated by (B) 20-cycle and (C) 10-cycle ALD-Al_2O_3. These cathodes were cycled at a current density of 240 mA/g over the voltage range of -0.3–0.8 V (vs. Ag/Ag^+). Reproduced with permission.[159] Copyright 2011, The Royal Society of Chemistry.

We conclude that the practice of depositing ALD coatings to modify both anodes and cathodes, as we discussed, clearly reveals several distinct benefits with this approach over conventional solution-based methods: (1) the uniform and conformal deposition of ultrathin films down to subnanometers; (2) successful deposition and growth of the coatings at low temperatures (typically less than 200 °C with possibility of going down to RT); (3) precise control of the coating films at the atomic level; (4) very facile operation; (5) a direct vapor deposition mode eliminating the need for solvents; (6) high quality films of the deposited coating materials; and, (7) high effectiveness in improving electrochemical performance comparable to those resulting from solution-based methods.

5. Concluding Remarks and Outlooks

As the most prevalent and promising energy storage devices, LIBs still face a series of challenges in cost, safety, energy density, and service life to secure their dominance in future transport usages. Recent advances in ALD demonstrated that it is a very useful tool for addressing these challenges, and also offers a variety of capabilities. On the one hand, recent studies showed that ALD is a flexible and tunable technique for synthesizing new LIB components covering anodes, cathodes, and inorganic solid electrolytes. On the other hand, research also revealed that ALD is a precise, highly efficient route to modify LIB electrodes with ultrathin surface coatings. Thus, ALD exhibited comprehensive superiorities over traditional methods in addressing the issues associated with LIBs. Within this context, we thoroughly reviewed the recent applications of ALD in LIBs, hoping to generate more interest in them and boosting extensive investigation in this emerging area.

We anticipate considerable advances in this emerging area because it imposes many new requirements on traditional ALD technologies, such as manufacturing abilities, material varieties, and characterization of ALD coatings. Thus, new vital interests are expected to motivate future studies.

5.1. Innovations of Conventional ALD Configurations

In traditional ALD systems, the ALD reactor is a fixed immobile flat chamber with a limited room. As a thin film technique, ALD is particularly suitable for the nanoscale film growth on bulk substrates such as Si wafers. Consequently, traditional ALD reactors are apparently deficient for assuring the mass production of powder-based nanomaterials, that is an essential requirement for large-sized LIBs in future HEVs, PHEVs, and EVs. Therefore, renovation must change the present

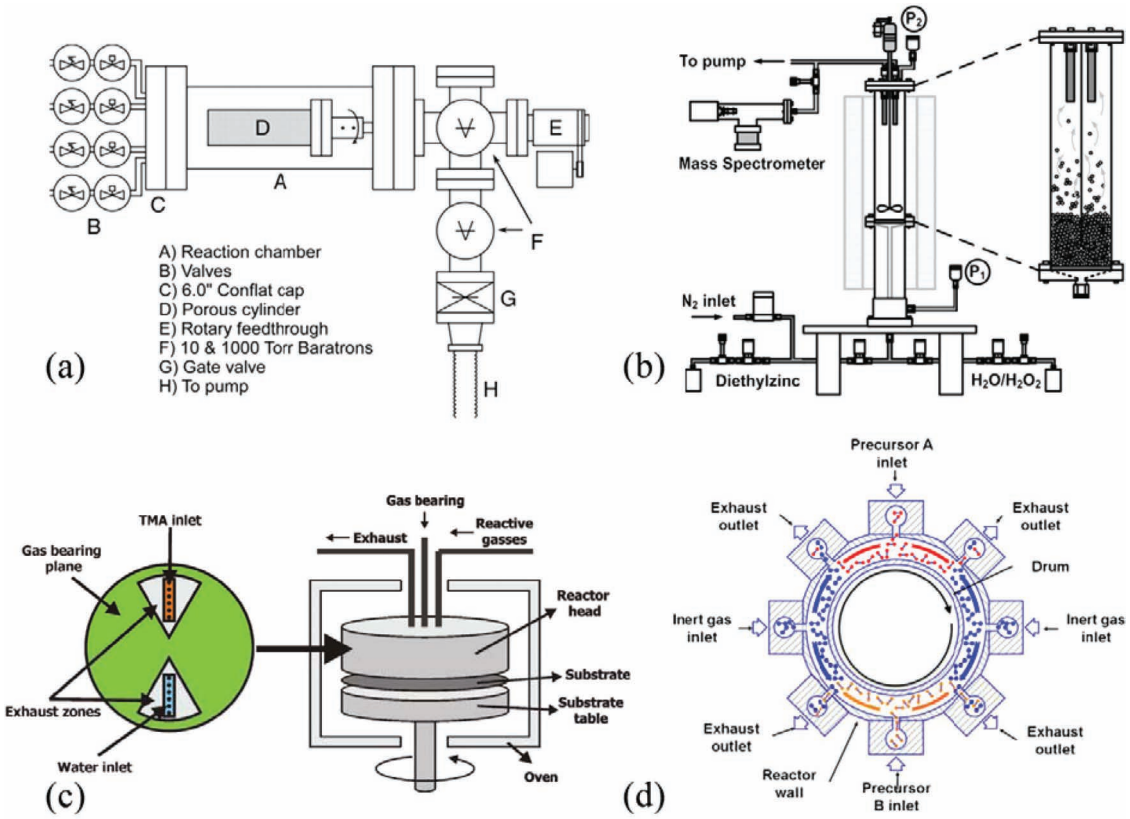

Figure 16. Innovative configurations of ALD systems: (a) rotary ALD reactor. Reproduced with permission.[180] Copyright 2009, Institute of Physics. (b) fluidized-bed ALD reactor. Reproduced with permission.[186] Copyright 2008, Elsevier. (c) and (d) high-speed and continuous spatial ALD reactors. Reproduced with permission[190]; Reproduced with permission.[193] Copyright 2011, Elsevier.

configurations of ALD reactors. In previous studies, two technical innovations were proposed for ALD reactors. One is based on a rotary reactor[178–182] and another employs the fluidized bed technology,[68,183–189] as illustrated in **Figure 16** (a) and (b), respectively. With the improved configuration of ALD reactors, the former ALD system was used for the processing of various nanomaterials, such as anoparticles,[178,179] MWCNTs,[180] graphene,[181] and polymer films/particles[182]. The latter ALD system was reported for the deposition of metal oxides on different nanoparticles.[68,183–189] The two technologies in essence increased the accommodation capabilities of ALD reactors. The maximum production of the two technologies is to date of the order of magnitude of grams, thus more effort is required to further raise their production capacity.

Meantime, new concepts were proposed for high-speed, continuous ALD[190–193] to improve the rapidity of traditional ALD processes. In conventional ALD processes, the deposition reaction is divided into two time-sequenced self-limiting half-reactions. In contrast, the new concepts spatially separate the half-reactions, as illustrated in Figure 16(c) and (d) with two new designs. In the two designs, substrates can rotate with adjustable speeds and one rotation is equivalent to one cycle of the ALD process. Thus, the new designs can quickly deposit films. In practice, the substrates receive precursors in different precursor zones that are spatially separated by purge zones and exhaust lines so precluding mixing of the gas phases between the precursors. Accordingly, the deposition rate is no longer limited by the accumulated times of the steps of individual cycles, but by the time required to form a monolayer. Al_2O_3, for example, reached 1.2 nm/s in a high speed spatial ALD in contrast to several hundredths of nm/s in traditional ALD-Al_2O_3.[192] The new designs can be used for rigid substrates (Figure 16(c)) and flexible substrates (Figure 16(d)). However, they are not suitable for powder-based materials.

5.2. Expanding Nanostructured Battery Components via ALD

In this review, it was demonstrated that ALD is a facile, versatile tool for designing and synthesizing nanostructured anodes, cathodes, and inorganic solid electrolytes. The resultant nanostructures can contribute to the development of better LIBs with improved performance such as energy density, safety, cost, and service life. However, so far, only a limited variety of materials have been investigated. For anode materials, for example, only the nanostructured anodes by ALD-TiO_2 and SnO_2 were evaluated electrochemically. Thus, other nanostructured materials of metals and metal oxides are expected to be investigated in future studies. Of them, we should pay greater attention to the nanostructures of high capacity materials such as Si and Sn. On the other hand, recent ALD work on lithium-containing ternary or more complex compounds[129–133] showed the feasibility

to develop another important anode material LTO. For cathodes, ALD to date has only succeeded in V_2O_5 nanofilms. Future studies are required to prepare other cathode materials, such as $LiCoO_2$, $LiMnO_2$, $LiMn_2O_4$, $LiNiO_2$, $LiNi_{0.5}Mn_{0.5}O_2$, $LiNi_{1/3}Mn_{1/3}Co_{1/3}O_2$, and $LiFePO_4$. In this scope, the recent successes[129–133] in lithium-containing films demonstrated that ALD is especially elegant at fine-tuning the compositions of complex compounds, implying the feasibility for synthesizing complex cathode materials. We noted the recent increase in interest for inorganic solid electrolytes, and many lithium containing films were developed. Future efforts are expected to bring more high efficient inorganic solid electrolytes (as reviewed by Thangadurai and Weppner,[29] and Xia et al.[30]) derived via ALD. With future successes in the three LIB components, ALD will help address the challenges facing LIBs.

5.3. Exploration on Multifunctional ALD Coatings

As reviewed in this work, surface coating via ALD represents a new high-quality surface modification of LIBs, offering the benefits of savings in both materials cost and processing time, and assuring the practicality of directly coating the electrodes. However, only a limited number of coating materials (Al_2O_3, TiO_2, ZnO, and TiN) were investigated. In the future, we expect that there will be available more varieties of coating materials for surface modification of LIB electrodes via ALD, such as metal oxides (e.g., MgO, ZrO_2, SnO_2, and B_2O_3), metal fluorides (e.g., AlF_3), metal oxyfluorides (e.g., BiOF), and other compounds. Electrode materials usually differ in their inherent properties, thus a coating material is expected to be selected exclusively for a specific electrode.

It is particularly important to address the roles and working mechanisms of the ALD-coatings so that we can develop LIBs more predictably. In this way, advanced characterization tools, especially in situ techniques are expected to play an essential part. Of a variety of in situ techniques, synchrotron-radiation (SR) based techniques are important for LIB studies, due to their capability to probe and deliver the information on the structures of electrodes and the complex interface of electrochemical systems during charge-discharge cycles. For example, in situ X-ray absorption spectroscopy (XAS) can be applied to determine atomic and electronic structure both of which are necessary to understand the relationships among atomic structure, electronic structure and electrochemical performance (including stability).[194] XAS requires only short-range order, so it provides structural information on amorphous solids, liquids, gases, and other complexes.[195] Interpreting all the spectra at different states of charge can afford us very useful quantitative and qualitative information on the valence change of the constituent elements in the electrode materials during the ongoing electrochemical reaction.[196] In situ high-resolution X-ray diffraction (XRD), another important tool, supports in situ studies of structural changes of LIB electrode materials,[194] that are essential to understand battery performance during charge-discharge cycles. Several excellent reviews have been previously conducted for the SR-based techniques in LIBs, by Marco and Veder,[194] McBreen,[195] and Deb and Cairns.[196] Our group at Brookhaven National Laboratory (BNL, New York, USA) has a long history of using the SR-based techniques in LIB studies for both anodes[197] and cathodes.[198–203] Our work demonstrated that SR-based in situ XRD and XAS could aid in addressing the effects of conventional coatings (such as Al_2O_3,[198] ZrO_2,[199–201] and C[197,202,203]) on electrochemical performance, and clarify the structures of various electrode materials. Thus, we believe that these techniques will be very helpful in delimiting the effects of ALD coatings on LIB performance.

Another advanced characterization technique is in situ HR-TEM that is garnering increasing attention for LIB research. Previously, this tool was used successfully for observing the graphitization of CNTs.[204] Recently, after the delivery of Huang's work[205] on characterizing the lithiation of SnO_2 nanowires, a series of important discoveries were reported on the structural changes of anode materials in lithiation or/and delithiation, including SnO_2 nanowires,[206] Si nanowires,[207] Ge nanowires,[208] ZnO nanowires,[209] and multi-walled CNTs.[210] The growth of lithium fibers on an anode was also recorded with in situ HR-TEM.[211] Using this technique, another group investigated the synthesis of carbon-coated $LiFePO_4$.[212] All these studies demonstrated that in situ HR-TEM is an invaluable tool for exploring the working mechanisms of LIBs. In particular, as we discussed in this review, Liu et al. attempted to clarify the roles of the Al_2O_3 coating for the lithiation-delithiation of Al nanowires.[149] In that work, as pointed out by the researchers, the naturally grown Al_2O_3 on Al nanowires were supposed to serve as the same functional roles as the ALD-Al_2O_3 coatings used in recent LIB studies. Thus, we believe that in situ HR-TEM will be very helpful in future LIB studies to clarify the roles and resulting mechanisms of ALD coatings.

In summary, recent studies demonstrated that ALD is a facile but versatile technique for developing high-performance LIBs. As an emerging area, the employment of ALD in LIBs deserves more extensive investigation in future studies.

Acknowledgements

This research at The University of Western Ontario was supported by the Natural Science and Engineering Research Council of Canada (NSERC), Canada Research Chair (CRC) Program, Canadian Foundation for Innovation (CFI), Ontario Research Fund (ORF), Early Researcher Award (ERA) and the University of Western Ontario. The work at Brookhaven National Laboratory was supported by NSERC Postdoctoral Fellowship, the US Department of Energy, the Assistant Secretary for Energy Efficiency and Renewable Energy, Office of Vehicle Technologies, under the program of Vehicle Technology Program, under Contract Number DEAC02-98CH10886. We thank Dr. Avril Woodhead for editing our article.

Received: January 28, 2012
Revised: March 22, 2012
Published online: June 15, 2012

[1] K. Tomabechi, *Energies* **2010**, *3*, 686.
[2] J. B. Goodenough, *J. Power Sources* **2007**, *174*, 996–1000.
[3] L.-X. Yuan, Z.-H. Wang, W.-X. Zhang, X.-L. Hu, J.-T. Chen, Y.-H. Huang, J. B. Goodenough, *Energy Environ. Sci.* **2011**, *4*, 269.
[4] M. S. Dresselhaus, I. L. Thomas, *Nature* **2001**, *414*, 332.
[5] M. R. Palacín, *Chem. Soc. Rev.* **2009**, *38*, 2565.

[6] Z. Yang, J. Zhang, M. C. W. Kintner-Meyer, X. Lu, D. Choi, J. P. Lemmon, J. Liu, *Chem. Rev.* **2011**, *111*, 3577.
[7] M. Armand, J.-M. Tarascon, *Nature* **2008**, *451*, 652.
[8] L. F. Nazar, G. Goward, F. Leroux, M. Duncan, H. Huang, T. Kerr, J. Gaubicher, *Int. J. Inorg. Mater.* **2001**, *3*, 191.
[9] J.-M. Tarascon, M. Armand, *Nature* **2001**, *414*, 359.
[10] B. Scrosati, J. Garche, *J. Power Sources* **2010**, *195*, 2419.
[11] J. B. Goodenough, Y. Kim, *Chem. Mater.* **2010**, *22*, 587.
[12] P. Arora, R. E. White, M. Doyle, *J. Electrochem. Soc.* **1998**, *145*, 3647.
[13] D. Aurbach, B. Markovsky, G. Salitra, E. Markevich, Y. Talyossef, M. Koltypin, L. Nazar, B. Ellis, D. Kovacheva, *J. Power Sources* **2007**, *165*, 491.
[14] Idaho National Laboratory, Battery test manual for plug-in hybrid electric vehicle: http://www.inl.gov, Accessed: June, **2010**.
[15] P. Poizot, S. Laruelle, S. Grugeon, L. Dupont, J.-M. Tarascon, *Nature* **2000**, *407*, 496.
[16] M. S. Whittingham, *Chem. Rev.* **2004**, *104*, 4271.
[17] A. S. Arico, P. Bruce, B. Scrosati, J.-M. Tarascon, W. V. Schalkwijk, *Nat. Mater.* **2005**, *4*, 366.
[18] D. Larcher, S. Beattie, M. Morcrette, K. Edström, J.-C. Jumas, J.-M. Tarascon, *J. Mater. Chem.* **2007**, *17*, 3759.
[19] Y. Wang, K. Takahashi, K. Lee, G. Cao, *Adv. Funct. Mater.* **2006**, *16*, 1133.
[20] Y. Wang, G. Cao, *Adv. Mater.* **2008**, *20*, 2251.
[21] Y.-G. Guo, J.-S. Hu, L.-J. Wan, *Adv. Mater.* **2008**, *20*, 2878.
[22] F. Cheng, Z. Tao, J. Liang, J. Chen, *Chem. Mater.* **2008**, *20*, 667.
[23] D. Deng, M. G. Kim, J. Y. Lee, J. Cho, *Energy Environ. Sci.* **2009**, *2*, 818.
[24] B. L. Ellise, K. T. Lee, L. F. Nazar, *Chem. Mater.* **2010**, *22*, 691.
[25] D. S. Su, R. Schlögl, *ChemSusChem.* **2010**, *3*, 136.
[26] H. Manjunatha, G. S. Suresh, T. V. Venkatesha, *J. Solid State Electrochem.* **2011**, *15*, 431.
[27] D. Baril, C. Michot, M. Armand, *Solid State Ionics* **1997**, *94*, 35.
[28] W. H. Meyer, *Adv. Mater.* **1998**, *10*, 439.
[29] V. Thangadurai, W. Weppner, *Ionics* **2006**, *12*, 81.
[30] H. Xia, H. L. Wang, W. Xiao, M. O. Lai, L. Lu, *Int. J. Surf. Sci. Eng.* **2009**, *3*, 23.
[31] P. Arora, Z. Zhang, *Chem. Rev.* **2004**, *104*, 4419.
[32] S. S. Zhang, *J. Power Sources* **2007**, *164*, 351.
[33] S. S. Zhang, *J. Power Sources* **2006**, *162*, 1379.
[34] L. J. Fu, H. Liu, C. Li, Y. P. Wu, E. Rahm, R. Holze, H. Q. Wu, *Solid State Sci.* **2006**, *8*, 113.
[35] C. Li, H. P. Zhang, L. J. Fu, H. Liu, Y. P. Wu, E. Rahm, R. Holze, H. Q. Wu, *Electrochim. Acta* **2006**, *51*, 3872.
[36] T.-F. Yi, Y.-R. Zhu, X.-D. Zhu, J. Shu, C.-B. Yue, A.-N. Zhou, *Ionics* **2009**, *15*, 779.
[37] S.-T. Myung, K. Amine, Y.-K. Sun, *J. Mater. Chem.* **2010**, *20*, 7074.
[38] Z. Chen, Y. Qin, K. Amine, Y.-K. Sun, *J. Mater. Chem.* **2010**, *20*, 7606.
[39] J. Wang, X. Sun, *Energy Environ. Sci.* **2012**, *5*, 5163.
[40] T. Suntola, J. Antson, **1977**, US patent 4058430.
[41] T. Suntola, *Mater. Sci. Rep.* **1989**, *4*, 261.
[42] H. Kim, *J. Vac. Sci. Technol. B* **2003**, *21*, 2231.
[43] A. C. Dillon, A. W. Ott, J. D. Way, S. M. George, *Surf. Sci.* **1995**, *322*, 230.
[44] J. E. Crowell, *J. Vac. Sci. Technol. A* **2003**, *21*, S88.
[45] R. L. Puurunen, *J. Appl. Phys.* **2005**, *97*, 121301.
[46] W. Gasser, Y. Uchida, M. Matsumura, *Thin Solid Films* **1994**, *250*, 213.
[47] A. Paranjpe, S. Gopinath, T. Omstead, R. Bubber, *J. Electrochm. Soc.* **2001**, *1486*, G465.
[48] M. Leskelä, M. Ritala, *Angew. Chem. Int. Ed.* **2003**, *42*, 5548.
[49] Y. Luo, D. Slater, M. Han, J. Moryl, R. M. Osgood, *Appl. Phys. Lett.* **1997**, *71*, 3799.
[50] J. W. Klaus, O. Sneh, S. M. George, *Science* **1997**, *278*, 1934.
[51] M. Putkonen, L. Niinistö, *Thin Solid Films* **2006**, *514*, 145.
[52] M. D. Groner, F. H. Fabreguette, J. W. Elam, S. M. George, *Chem. Mater.* **2004**, *16*, 639.
[53] M. Knez, A. Kadri, C. Wege, U. Gösele, H. Jeske, K. Nielsch, *Nano Lett.* **2006**, *6*, 1172.
[54] Y.-M. Chang, S.-R. Jian, H.-Y. Lee, C.-M. Lin, J.-Y. Juang, *Nanotechnology* **2010**, *21*, 385705.
[55] B. H. Lee, S. Cho, J. K. Hwang, S. H. Kim, M. M. Sung, *Thin Solid Films* **2010**, *518*, 6432.
[56] J. Heo, A. S. Hock, R. G. Gordon, *Chem. Mater.* **2010**, *22*, 4964.
[57] B. H. Lee, J. K. Hwang, J. W. Nam, S. U. Lee, J. T. Kim, S.-M. Koo, A. Baunemann, R. A. Fisher, M. M. Sung, *Angew. Chem. Int. Ed.* **2009**, *48*, 4536.
[58] G. A. Ten Eyck, S. Pimanpang, H. Bakhru, T.-M. Lu, G.-C. Wang, *Chem. Vap. Deposition* **2006**, *12*, 290.
[59] K Kukli, M. Ritala, M. Leskelä, J. Jokinen, *J. Vac. Sci. Technol. A* **1997**, *15*, 2214.
[60] C.-W. Jeong, B.-i. Lee, S.-K. Joo, *Mater. Sci. Eng. C* **2001**, *16*, 59.
[61] D. Hausmann, J. Becker, S. Wang, R. G. Gordon, *Science* **2002**, *298*, 402.
[62] J. Niinistö, N. Petrova, M. Putkonen, L. Niinistö, K. Arstila, T. Sajavaara, *J. Cryst. Growth* **2005**, *285*, 191.
[63] K. Kukli, M. Ritala, M. Leskelä, T. Sajavaara, J. Keinonen, D. C. Gilmer, R. Hegde, R. Rai, L. Prabhu, *J. Mater. Sci.* **2003**, *14*, 361.
[64] A. W. Ott, K. C. McCarley, J. W. Klaus, J. D. Way, S. M. George, *Appl. Surf. Sci.* **1996**, *107*, 128.
[65] A. W. Ott, J. W. Klaus, J. M. Johnson, S. M. George, *Thin Solid Films* **1997**, *292*, 135.
[66] S. S. Lee, J. Y. Baik, K.-S An, Y. D. Suh, J.-H Oh, Y. Kim, *J. Phys. Chem. B* **2004**, *108*, 15128.
[67] J. W. Elam, Z. A. Sechrist, S. M. George, *Thin Solid Films* **2002**, *414*, 43.
[68] X. Liang, K. S. Barrett, Y.-B. Jiang, A. W. Weimer, *ACS Appl. Mater. Interfaces* **2010**, *2*, 2248.
[69] T. H. Han, H.-S. Moon, J. O. Hwang, S. I. Seok, S. H. Im, S. O. Kim, *Nanotechnology* **2010**, *21*, 185601.
[70] D. Gu, H. Baumgart, T. M. Abdel-Fattah, G. Namkoong, *ACS Nano* **2010**, *4*, 753.
[71] E. R. Cleveland, P. Banerjee, I. Perez, S. B. Lee, G. W. Rubloff, *ACS Nano* **2010**, *4*, 4637.
[72] A. Brzezinski, Y.-C. Chen, P. Wiltzius, P. V. Braun, *J. Mater. Chem.* **2009**, *19*, 9126.
[73] M. Knez, K. Nielsch, L. Niinistö, *Adv. Mater.* **2007**, *19*, 3425.
[74] H. Kim, H.-B.-R. Lee, W.-J. Maeng, *Thin Solid Films* **2009**, *517*, 2563.
[75] S. M. George, *Chem. Rev.* **2010**, *110*, 111.
[76] P. Verma, P. Maire, P. Novák, *Electrochim. Acta* **2010**, *55*, 6332.
[77] S. K. Cheah, E. Perre, M. Rooth, M. Fondell, A. Hårsta, L. Nyholm, M. Boman, T. Gustafsson, J. Lu, P. Simon, K. Edström, *Nano Lett.* **2009**, *9*, 3230.
[78] C. J. W. Ng, H. Gao, T. T. Y. Tan, *Nanotechnology* **2008**, *19*, 445604.
[79] L. K. Tan, M. A. S. Chong, H. Gao, *J. Phys. Chem. C* **2008**, *112*, 69.
[80] L. K. Tan, H. Gao, Y. Zong, W. Knoll, *J. Phys. Chem. C* **2008**, *112*, 17576.
[81] Y.-H. Chang, C.-M. Liu, Y.-C. Tseng, C. Chen, C.-C. Chen, H.-E. Cheng, *Nanotechnology* **2010**, *21*, 225602.
[82] L. K. Tan, M. K. Kumar, W. W. An, H. Gao, *ACS Appl. Mater. Interfaces* **2010**, *2*, 498.
[83] C.-M. Liu, C. Chen, H.-E. Cheng, *J. Electrochm. Soc.* **2011**, *158*, K58.
[84] C.-M. Liu, C. Chen, H.-E. Cheng, *Electrochem Solid State Lett.* **2011**, *14*, K33.

[85] J. T. Korhonen, P. Hiekkataipale, J. Malm, M. Karppinen, O. Ikkala, R. H. A. Ras, *ACS Nano* **2011**, *5*, 1967.
[86] M. Rooth, R. A. Quinlan, E. Widenkvist, J. Lu, H. Grennberg, B. C. Holloway, A. Hårsta, U. Jansson, *J. Cryst. Growth* **2009**, *311*, 373.
[87] K. Gerasopoulos, X. Chen, J. Culver, C. Wang, R. Ghodssi, *Chem. Commun.* **2010**, *46*, 7349.
[88] C. Bae, S. Kim, B. Ahn, J. Kim, M. M. Sung, H. Shin, *J. Mater. Chem.* **2008**, *18*, 1362.
[89] J. Lee, H. Ju, J. K. Lee, H. S. Kim, J. Lee, *Electrochem. Commun.* **2010**, *12*, 210.
[90] H. Shin, D.-K. Jeong, J. Lee, M. M. Sung, J. Kim, *Adv. Mater.* **2004**, *16*, 1197.
[91] X. Meng, D. Geng, J. Liu, R. Li, X. Sun, *Nanotechnology* **2011**, *22*, 165602.
[92] T. H. Han, J. K. Oh, J. S. Park, S.-H. Kwon, S.-W. Kim, S. O. Kim, *J. Mater. Chem.* **2009**, *19*, 3512.
[93] S.-W. Kim, T. H. Han, J. Kim, H. Gwon, H.-S. Moon, S.-W. Kang, S. O. Kim, K. Kang, *ACS Nano* **2009**, *3*, 1085.
[94] M. Rooth, A. Johansson, K. Kukli, J. Aarik, M. Boman, A. Hårsta, *Chem. Vap. Deposition* **2008**, *14*, 67.
[95] X. Meng, M. Ionescu, M. N. Banis, Y. Zhong, H. Liu, Y. Zhang, S. Sun, R. Li, X. Sun, *J. Nanopart. Res.* **2011**, *13*, 1207.
[96] J. Bachmann, J. Jing, M. Knez, S. Barth, H. Shen, S. Mathur, U. Gosele, K. Nielsch, *J. Am. Chem. Soc.* **2007**, *129*, 9554.
[97] Y.-S. Min, E. J. Bae, J. B. Park, U. J. Kim, W. Park, J. Song, C. S. Hwang, N. Park, *Appl. Phys. Lett.* **2007**, *90*, 263104.
[98] D. S. Kim, S.-M. Lee, R. Scholz, M. Knez, U. Gösele, J. Fallert, H. Kalt, M. Zacharias, *Appl. Phys. Lett.* **2008**, *93*, 103108.
[99] Y.-H. Lin, P.-S. Lee, Y.-C. Hsueh, K.-Y. Pan, C.-C. Kei, M.-H. Chan, J.-M. Wu, T.-P. Perng, H. C. Shih, *J. Electrochem. Soc.* **2011**, *158*, K24.
[100] A. B. F. Martinson, J. W. Elam, J. T. Hupp, M. J. Pellin, *Nano Lett.* **2007**, *7*, 2183.
[101] Y.-H. Chang, S.-M. Wang, C.-M. Liu, C. Chen, *J. Electrochem. Soc.* **2010**, *157*, K236.
[102] X. Meng, Y. Zhang, S. Sun, R. Li, X. Sun, *J. Mater. Chem.* **2011**, *21*, 12321.
[103] X. Meng, Y. Zhong, Y. Sun, M. N. Banis, R. Li, X. Sun, *Carbon.* **2011**, *49*, 1133.
[104] X. Meng, D. Geng, J. Liu, M. N. Banis, Y. Zhang, R. Li, X. Sun, *J. Phys. Chem. C* **2010**, *114*, 18330.
[105] W.-S. Kim, B.-S. Lee, D.-H. Kim, H.-C. Kim, W.-R. Yu, S.-H. Hong, *Nanotechnology* **2010**, *21*, 245605.
[106] C. Marichy, N. Donato, M.-G. Willinger, M. Latino, D. Karpinsky, S.-H. Yu, G. Neri, N. Pinna, *Adv. Funct. Mater.* **2011**, *21*, 658.
[107] K. S. Novoselov, A. K. Geim, S. V. Morozov, D. Jiang, Y. Zhang, S. V. Dubonos, I. V. Grigorieva, A. A. Firsov, *Science* **2004**, *306*, 666.
[108] K. I. Bolotin, K. J. Sikes, Z. Jiang, M. Klima, G. Fudenberg, J. Hone, P. Kim, H. L. Stormer, *Solid State Commun.* **2008**, *146*, 351.
[109] M. D. Stoller, S. Park, Y. Zhu, J. An, R. S. Ruoff, *Nano Lett.* **2008**, *8*, 3498.
[110] D. Wang, D. Choi, J. Li, Z. Yang, Z. Nie, R. Kou, D. Hu, C. Wang, L. V. Saraf, J. Zhang, I. A. Aksay, J. Liu, *ACS Nano* **2009**, *3*, 907.
[111] S. M. Paek, E. Yoo, I. Honma, *Nano Lett.* **2009**, **9**, 72.
[112] E. Perre, L. Nyholm, T. Gustfsson, P.-L. Taberna, P. Simon, K. Edström, *Electrochem. Commun.* **2008**, *10*, 1467.
[113] X. Li, X. Meng, J. Liu, D. Geng, Y. Zhang, M. N. Banis, Y. Li, R. Li, X. Sun, M. Cai, M. W. Verbrugge, *Adv. Funct. Mater.* **2012**, 22, 1647.
[114] K. Mizushima, P. C. Jones, P. J. Wiseman, J. B. Goodenough, *Mat. Res. Bull.* **1980**, *15*, 783.
[115] M. M. Thackeray, W. I. F. David, P. G. Bruce, J. B. Goodenough, *Mat. Res. Bull.* **1983**, *18*, 461.
[116] A. Patil, V. Patil, D. W. Shin, J.-W. Choi, D.-S. Paik, S.-J. Yoon, *Mater. Res. Bull.* **2008**, *43*, 1913.
[117] S. Beke, *Thin Solid Films.* **2011**, *519*, 1761.
[118] M. S. Whittingham, *J. Electrochem. Soc.* **1976**, *123*, 315.
[119] M. Baba, N. Kumagai, H. Kobayashi, O. Nakano, K. Nishidate, *Electrochem. Solid State Lett.* **1999**, *2*, 320.
[120] J. C. Badot, S. Ribes, E. B. Yousfi, V. Vivier, J. P. Pereira-Ramos, N. Baffier, D. Lincot, *Electrochem. Solid State Lett.* **2000**, *3*, 485.
[121] J. C. Badot, A. Mantoux, N. Baffier, O. Dubrunfaut, D. Lincot, *J. Mater. Chem.* **2004**, *14*, 3411.
[122] R. Baddour-Hadjean, V. Golabkan, J. P. Pereira-Ramos, A. Mantoux, D. Lincot, *J. Raman Spectrosc.* **2002**, *33*, 631.
[123] K. Le Van, H. Groult, A. Mantoux, L. Perrigaud, F. Lantelme, R. Lindström, R. Badour-Hadjean, S. Zanna, D. Lincot, *J. Power Sources* **2006**, *160*, 592.
[124] N. Ohta, K. Takada, L. Zhang, R. Ma, M. Osada, T. Sasaki, *Adv. Mater.* **2006**, *18*, 2226.
[125] L. Baggetto, R. A. H. Niessen, F. Roozeboom, P. H. L. Notten, *Adv. Funct. Mater.* **2008**, *18*, 1057.
[126] J. W. Long, B. Dun, D. R. Rolison, H. S. White, *Chem. Rev.* **2004**, *104*, 4463.
[127] M. Roberts, P. Johns, J. Owen, D. Brandell, K. Edstrom, G. E. Enany, C. Guery, D. Golodnitsky, M. Lacey, C. Lecoeur, H. Mazor, E. Peled, E. Perre, M. M. Shaijumon, P. Simon, P.-L. Taberna, *J. Mater. Chem.* **2011**, *21*, 9876.
[128] P. H. L. Notten, F. Roozeboom, R. A. H. Niessen, L. Baggetto, *Adv. Mater.* **2007**, *19*, 4564.
[129] M. Putkonen, T. Aaltonen, M. Alnes, T. Sajavaara, O. Nilsen, H. Fjellvåg, *J. Mater. Chem.* **2009**, *19*, 8767.
[130] T. Aaltonen, M. Alnes, O. Nisen, L. Costelle, H. Fjellvåg, *J. Mater. Chem.* **2010**, *20*, 2877.
[131] T. Aaltonen, O. Nisen, A. Magrasó, H. Fjellvåg, *Chem. Mater.* **2011**, *23*, 4669.
[132] Y.-C. Perng, J. Cho, D. Membreno, B. Dunn, M. F. Toney, J. P. Chang, 11th International Conference on Atomic Layer Deposition, (Jun. 26–29) **2011**, Cambridge, MA, USA.
[133] J. Hämäläinen, T. Hatanpää, J. Holopainen, F. Munnik, M. Ritala, M. Leskelä, 11th International Conference on Atomic Layer Deposition, (Jun. 26–29) **2011**, Cambridge, MA, USA.
[134] K. Xu, *Energies* **2010**, *3*, 135.
[135] M. Winter, *Z. Phys. Chem.* **2009**, *223*, 1395.
[136] Y. S. Jung, A. S. Cavanagh, L. A. Riley, S.-H. Kang, A. C. Dillon, M. D. Groner, S. M. George, S.-H. Lee, *Adv. Mater.* **2010**, *22*, 2172.
[137] I. Lahiri, S.-M. Oh, J. Y. Hwang, C. Kang, M. Choi, H. Jeon, R. Banerjee, Y.-K. Sun, W. Choi, *J. Mater. Chem.* **2011**, *21*, 13621.
[138] L. A. Riley, A.S. Cavanagh, S. M. George, Y. S. Jung, Y. Yan, S.-H. Lee, A. C. Dillon, *ChemPhysChem.* **2010**, *11*, 2124.
[139] L. A. Riley, A. S. Cavanagh, S. M. George, S.-H. Lee, A. C. Dillon, *Electrochem. Solid State Lett.* **2011**, *14*, A29.
[140] E. Kang, Y. S. Jung, A. S. Cavanagh, G.-H. Kim, S. M. George, A. C. Dillon, J. K. Kim, J. Lee, *Adv. Funct. Mater.* **2011**, *21*, 2430.
[141] D. Ahn, X. Xiao, *Electrochem. Commun.* **2011**, *13*, 796.
[142] X. Xiao, P. Lu, D. Ahn, *Adv. Mater.* **2011**, *23*, 3911.
[143] Y. He, X. Yu, Y. Wang, H. Li, X. Huang, *Adv. Mater.* **2011**, *23*, 4938.
[144] J.-H. Lee, M.-H. Hon, Y.-W. Chung, I.-C. Leu, *Appl. Phys. A.* **2011**, *102*, 545.
[145] M. Q. Snyder, S. A. Trebukhova, B Ravdel, M. C. Wheeler, J. DiCarlo, C. P. Tripp, W. J. DeSisto, *J. Power Sources* **2007**, *165*, 379.
[146] I. Lahiri, S.-M. Oh, J. Y. Hwang, S. Cho, Y.-K. Sun, R. Banerjee, W. Choi, *ACS Nano* **2010**, *4*, 3440.
[147] K. Leung, Y. Qi, K. R. Zavadil, Y. S. Jung, A. C. Dillon, A. S. Cavanagh, S.-H. Lee, S. M. George, *J. Am. Chem. Soc.* **2011**, *133*, 14741.
[148] M. I. Dafinone, G. Feng, T. Brugarolas, K. E. Tettey, D. Lee, *ACS Nano* **2011**, *5*, 5078.

[149] Y. Liu, N. S. Hudak, D. L. Huber, S. J. Limmer, J. P. Sullivan, J. Y. Huang, *Nano Lett.* **2011**, *11*, 4188.
[150] F. Belliard, J. T. S. Irvine, *J. Power Sources* **2001**, *97–98*, 219.
[151] J. Liu, Y. Li, R. Ding, J. Jiang, Y. Hu, X. Ji, Q. Chi, Z. Zhu, X. Huang, *J. Phys. Chem. C.* **2009**, *113*, 5336.
[152] T.-F. Yi, L.-J. Jiang, J. Shu, C.-B. Yue, R.-S. Zhu, H.-B. Qiao, *J. Phys. Chem. Solids* **2010**, *71*, 1236.
[153] H.-Q. Gao, X.-Y. Wang, Z.-A. Zhang, Y.-Q. Lai, J. Li, Y.-X. Liu, *J. Inorg. Mater.* **2010**, *25*, 983.
[154] G. G. Amatucci, J.-M. Tarascon, **1998**, US Patent 5705291.
[155] Y.-S. Jung, A. S. Cavanagh, A. C. Dillon, M. D. Groner, S. M. George, S.-H. Lee, *J. Electrochem. Soc.* **2010**, *157*, A75.
[156] J.-T. Lee, F.-M. Wang, C.-S. Cheng, C.-C. Li, C.-H. Lin, *Electrochim. Acta* **2010**, *55*, 4002.
[157] I. D. Scott, Y. S. Jung, A. S. Cavanagh, Y. Yan, A. C. Dillon, S. M. George, S.-H. Lee, *Nano Lett.* **2011**, *11*, 414.
[158] L. A. Riley, S. V. Atta, A. S. Cavanagh, Y. Yan, S. M. George, P. Liu, A. C. Dillon, S.-H. Lee, *J. Power Sources* **2011**, *196*, 3317.
[159] D. Guan, J. A. Jeevarajan, Y. Wang, *Nanoscale* **2011**, *3*, 1465.
[160] L. Liu, Z. Wang, H. Li, L. Chen, X. Huang, *Solid State Ionics* **2002**, *152–153*, 341.
[161] G. T.-K. Fey, C.-Z. Lu, J.-D. Huang, T. P. Kumar, Y.-C. Chang, *J. Power Sources* **2005**, *146*, 65.
[162] G. T.-K. Fey, P. Muralidharan, C.-Z. Lu, Y.-D. Cho, *Electrochim. Acta* **2006**, *51*, 4850.
[163] Q. Cao, H. P. Zhang, G. J. Wang, Q. Xia, Y. P. Wu, H. Q. Wu, *Electrochem. Commun.* **2007**, *9*, 1228.
[164] G. T.-K. Fey, C.-F. Huang, P. Muralidharan, E. S.-S. Chang, *J. Power Sources* **2007**, *174*, 1147.
[165] C.-Z. Lu, J.-M. Chen, Y.-D. Cho, W.-H. Hsu, P. Muralidharan, G. T.-K. Fey, *J. Power Sources* **2008**, *184*, 392.
[166] T. Ohzuku, Y. Makimura, *Chem. Lett.* **2001**, *30*, 642.
[167] F. Wu, M. Wang, Y. Su, S. Chen, *J. Power Sources* **2009**, *189*, 743.
[168] H.-Y. Wang, A.-D. Tang, K.-L. Huang, S.-Q. Liu, *Trans. Nonferrous Met. Soc. China* **2010**, *20*, 803.
[169] Z. Yang, X.-H. Li, Z.-X. Wang, Y.-J. Zhu, *Trans. Nonferrous Met. Soc. China* **2007**, *17*, 1319.
[170] G. T.-K. Fey, C.-S. Chang, T. P. Kumar, *J. Solid State Electrochem.* **2010**, *14*, 17.
[171] X. M. Wu, S. Chen, M. Y. Ma, J. B. Liu, *Ionics* **2011**, *17*, 35.
[172] J. Tu, X. B. Zhao, G. S. Cao, J. P. Tu, T. J. Zhu, *Mater. Lett.* **2006**, *60*, 3251.
[173] S.-W. Lee, K.-S. Kim, H.-S. Moon, H.-J. Kim, B.-W. Cho, W.-I. Cho, J.-B. Ju, J.-W. Park, *J. Power Sources* **2004**, *126*, 150.
[174] L. Yu, X. Qiu, J. Xi, W. Zhu, L. Chen, *Electrochim. Acta* **2006**, *51*, 6406.
[175] C. Lai, W. Ye, H. Liu, W. Wang, *Ionics* **2009**, *15*, 389.
[176] D. Liu, X. Liu, Z. He, *J. Alloy. Comp.* **2007**, *436*, 387.
[177] H. Sahan, H. Goktepe, S. Patat, A. Ulgen, *Solid State Ionics* **2010**, *181*, 1437.
[178] J. A. McCormick, B. L. Cloutier, A. W. Weimer, S. M. George, *J. Vac. Sci. Technol. A* **2007**, *25*, 67.
[179] J. A. McCormick, K. P. Rice, D. F. Paul, A. W. Weimer, S. M. George, *Chem. Vap. Deposition* **2007**, *13*, 491.
[180] A. S. Cavanagh, C. A. Wilson, A. W. Weimer, S. M. George, *Nanotechnology* **2009**, *20*, 255602.
[181] X. Sun, M. Xie, G. Wang, H. Sun, A. S. Cavanagh, J. J. Travis, S. M. George, J. Lian, *J. Electrochem. Soc.* **2012**, *159*, A364.
[182] C. A. Wilson, J. A. McCormick, A. S. Cavanagh, D. N. Goldstein, A. W. Weimer, S. M. George, *Thin Solid Films* **2008**, *516*, 6175.
[183] J. R. Wank, S. M. George, A. W. Weimer, *J. Am. Ceram. Soc.* **2004**, *87*, 762.
[184] L. F. Hakim, J. Blackson, S. M. George, A. W. Weimer, *Chem. Vap. Deposition* **2005**, *11*, 420.
[185] X. Liang, G.-D. Zhan, D. M. King, J. A. McCormick, J. Zhang, S. M. George, A. W. Weimer, *Diamond Relat. Mater.* **2008**, *17*, 185.
[186] D. M. King, X. Liang, Y. Zhou, C. S. Carney, L. F. Hakim, P. Li, A. W. Weimer, *Powder Technol.* **2008**, *183*, 356.
[187] D. M. King, X. Liang, C. S. Carney, L. F. Hakim, P. Li, A. W. Weimer, *Adv. Funct. Mater.* **2008**, *18*, 607.
[188] D. M. King, X. Liang, P. Li, A. W. Weimer, *Thin Solid Films* **2008**, *516*, 8517.
[189] J. R. Scheffe, A. Francés, D. M. King, X. Liang, B. A. Branch, A. S. Cavanagh, S. M. George, A. W. Weimer, *Thin Solid Films.* **2009**, *517*, 1874.
[190] P. Poodt, A. Lankhorst, F. Roozeboom, K. Spee, D. Maas, A. Vermeer, *Adv. Mater.* **2010**, *22*, 3564.
[191] P. Poodt, V. Tiba, F. Werner, J. Schmidt, A. Vermeer, F. Roozeboom, *J. Electrochem. Soc.* **2011**, *158*, H937.
[192] B. Vermang, A. Rothschild, A. Racz, J. John, J. Poortmans, R. Mertens, P. Poodt, V. Tiba, F. Roozeboom, *Prog. Photovolt: Res. Appl.* **2011**, *19*, 733.
[193] P. S. Maydannik, T. O. Kääriäinen, D. C. Cameron, *Chem. Eng. J.* **2011**, *171*, 345.
[194] R. D. Marco, J.-P. Veder, *TrAC, Trends Anal. Chem.* **2010**, *29*, 528.
[195] J. McBreen, *J. Solid State Electrochem.* **2009**, *13*, 1051.
[196] A. Deb, E. J. Cairns, *Fluid Phase Equilib.* **2006**, *241*, 4.
[197] X.-Q. Yang, J. McBreen, W.-S. Yoon, M. Yoshio, H. Wang, K. Fukuda, T. Umeno, *Electrochem. Commun.* **2002**, *4*, 893.
[198] L. Liu, L. Chen, X. Huang, X.-Q. Yang, W.-S. Yoon, H. S. Lee, J. McBreen, *J. Electrochem. Soc.* **2004**, *151*, A1344.
[199] K. Y. Chung, W.-S. Yoon, H. S. Lee, J. McBreen, X.-Q. Yang, S. H. Oh, W. H. Ryu, J. L. Lee, W. I. Cho, B. W. Cho, *J. Power Sources* **2006**, *163*, 185.
[200] K. Y. Chung, W.-S. Yoon, J. McBreen, X.-Q. Yang, S. H. Oh, H. C. Shin, W. I. Cho, B. W. Cho, *J. Electrochem. Soc.* **2006**, *153*, A2152.
[201] K. Y. Chung, W.-S. Yoon, J. McBreen, X.-Q. Yang, S. H. Oh, H. C. Shin, W. I. Cho, B. W. Cho, *J. Power Sources* **2007**, *174*, 619.
[202] K.-W. Nam, X.-J. Wang, W.-S. Yoon, H. Li, X. Huang, O. Haas, J. Bai, X.-Q. Yang, *Electrochem. Commun.* **2009**, *11*, 913.
[203] H. C. Shin, K. W. Nam, W. Y. Chang, B. W. Cho, W.-S. Yoon, X.-Q. Yang, K. Y. Chung, *Electrochim. Acta* **2011**, *56*, 1182.
[204] A. Yasuda, N. Kawase, F. Banhart, W. Mizutani, T. Shimizu, H. Tokumoto, *J. Phys. Chem. B* **2002**, *106*, 1894.
[205] J. Y. Huang, L. Zhong, C. M. Wang, J. P. Sullivan, W. Xu, L. Q. Zhang, S. X. Mao, N. S. Hudak, X. H. Liu, A. Subramanian, H. Fan, L. Qi, A. Kushima, J. Li, *Science* **2010**, *330*, 1515.
[206] L. Zhong, X. H. Liu, G. F. Wang, S. X. Mao, J. Y. Huang, *Phys. Rev. Lett.* **2011**, *106*, 248302.
[207] X. H. Liu, H. Zheng, L. Zhong, S. Huang, K. Karki, L. Q. Zhang, Y. Liu, A. Kushima, W. T. Liang, J. W. Wang, J.-H. Cho, E. Epstein, S. A. Dayeh, S. T. Picraux, T. Zhu, J. Li, J. P. Sullivan, J. Cumings, C. Wang, S. X. Mao, Z. Z. Ye, S. Zhang, J. Y. Huang, *Nano Lett.* **2011**, *11*, 3312.
[208] X. H. Liu, S. Huang, S. T. Picraux, J. Li, T. Zhu, J. Y. Huang, *Nano Lett.* **2011**, *11*, 3991.
[209] A. Kushima, X. H. Liu, G. Zhu, Z. L. Wang, J. Y. Huang, J. Li, *Nano Lett.* **2011**, *11*, 4535.
[210] Y. Liu, H. Zheng, X. H. Liu, S. Huang, T. Zhu, J. Wang, A. Kushima, N. S. Hudak, X. Huang, S. Zhang, S. X. Mao, X. Qian, J. Li, J. Y. Huang, *ACS Nano* **2011**, *5*, 7245.
[211] X. H. Liu, L. Zhong, L. Q. Zhang, A. Kushima, S. X. Mao, J. Li, Z. Z. Ye, J. P. Sullivan, J. Y. Huang, *Appl. Phys. Lett.* **2011**, *98*, 183107.
[212] M. L. Trudeau, D. Laul, R. Veillette, A. M. Serventi, A. Mauger, C. M. Julien, K. Zaghib, *J. Power Sources* **2011**, *196*, 7383.